Investigation of Polymer Nano-coatings for the Durability Improvement of Heat Exchanger

Dissertation

Submitted in partial fulfilment of the requirement for the award of the degree of

Master of Engineering

in

Thermal Engineering

by

Rishav Kumar

Registration No.: 802083010

Under the Supervision of

Dr. Deepak Jain
Associate Professor, MED
Thapar Institute of Engineering and Technology, Patiala

Dr. Kundan Lal
Assistant Professor, MED
Thapar Institute of Engineering and Technology, Patiala

Department of Mechanical Engineering

Thapar Institute of Engineering & Technology

(Deemed to be University)

CERTIFICATE OF DECLARATION

I hereby certify that the dissertation entitled **"Investigation of polymer nano-coatings for the durability improvement of heat exchanger"** contains my bonafide work carried out in completing the project requirement for the degree of Master of Engineering in Thermal Engineering at Thapar Institute of Engineering and Technology under the guidance of Dr. Deepak Jain, Associate Professor, and Dr. Kundan Lal, Assistant Professor in the Department of Mechanical Engineering, Thapar Institute of Engineering and Technology, Patiala.

It is certified that the above statement made by the student is correct to the best of my knowledge and belief.

Rishav Kumar

Roll No. 802083010

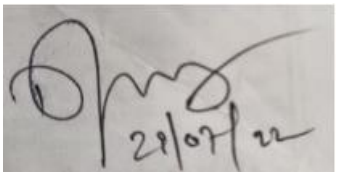

Dr. Deepak Jain
Associate Professor, MED
Thapar Institute of Engineering and Technology, Patiala

Dr. Kundan Lal
Assistant Professor, MED
Thapar Institute of Engineering and Technology, Patiala

ACKNOWLEDGEMENT

I would like to express my profound gratitude to all those who have been instrumental in the completion of this thesis. I wish to express my deep sense of gratitude and sincere appreciation to my supervisors **Dr. Deepak Jain,** Associate Professor, Department of Mechanical Engineering, and **Dr. Kundan Lal,** Assistant professor, Department of Mechanical Engineering for their continuous support, advice, and encouragement, without which this study could never have been completed.

I am incredibly thankful to **Prof. Prakash Gopalan**, Director, Thapar Institute of Engineering and Technology (Deemed to be University), and **Dr. T.K. Bera,** Head, Department of Mechanical Engineering, Thapar Institute of Engineering and Technology (Deemed to be University) for allowing me to undertake this research work.

I would like to thank **Dr. Bikramjit Sharma,** Assistant professor, Department of Mechanical Engineering, and **Mr. Nikhil Sharma,** JRF for providing me with all the necessary help I required. Finally, I would like to thank my family for their endless support and understanding of my goals and aspirations.

ABSTRACT

Industries are facing a major problem due to the deposition of the scaling/fouling layer on the plate heat exchanger which directly affects the life expectancy of the heat exchangers. The buildup of scaling/fouling layers over the surface of the heat exchangers also reduces the cross-sectional area of the tubes or flow channels, which increases the resistance of the passing fluid. To mitigate the scaling/fouling problem in the heat exchangers, coatings are the prevalent, practical, and preferred method to protect the metals like stainless steel and its alloys from corrosion. In this era, graphene-based organic polymer coatings are widely used as corrosion fortification aids. Graphene has engrossed momentous responsiveness in several industrial fields due to its greater anti-corrosion and barrier properties. In the present study, the graphene-based epoxy polymer coating was applied on SS304 grade using the paint spray technique. Several heat transfer effectiveness experiments were conducted on the heat exchanger test rig. The coatings were characterized using FE-SEM and Raman spectroscopy to confirm the uniform distribution of graphene. Potentiodynamic polarization tests were conducted on the specimen to evaluate the anti-corrosion performance of the coating. FE-SEM and Raman spectroscopy results showed that the spray coating technique is suitable. Electrochemical results reveal that the graphene-based epoxy polymer coating is ~18% less corrosive than the SS304 grade. The incorporation of 0.3 wt.% of graphene into the epoxy coating significantly improved the corrosion resistance and thermal properties.

Keywords: *Heat exchanger, epoxy coatings, graphene coatings, potentiodynamic polarization, FE-SEM, etc.*

TABLE OF CONTENT

LIST OF FIGURE

LIST OF TABLES

CHAPTER 1

Introduction

This section has covered the introduction to heat exchangers, corrosion, fouling losses, and modern-day techniques to avoid fouling. Furthermore, this section also comprises the requirements, inspiration, benefits, and applications of recent work.

1.1 Heat Exchanger

A heat exchanger is a type of mechanical device that helps to exchange the heat of cool fluid for hot fluid or vice versa. Heat exchangers are widely used in industrial as well as domestic applications. The most common types of heat exchangers are concurrent or parallel flow, counter-flow, single-pass crossflow, and multi-pass crossflow [1]. All type of heat exchanger works on constant pressure e.g. evaporator, condenser, boilers, etc.

Types of Heat Exchangers

1. Simple Heat Exchanger

In a simple heat exchanger, there are two concentric pipes with different radii. Two arrangements are possible in this type of heat exchanger i.e. parallel flow and counter-flow. In parallel flow, both hot fluid and cold fluid enter from the same end and flow in the same direction. In counter-flow both fluids enter from opposite ends and also flows in opposite direction.

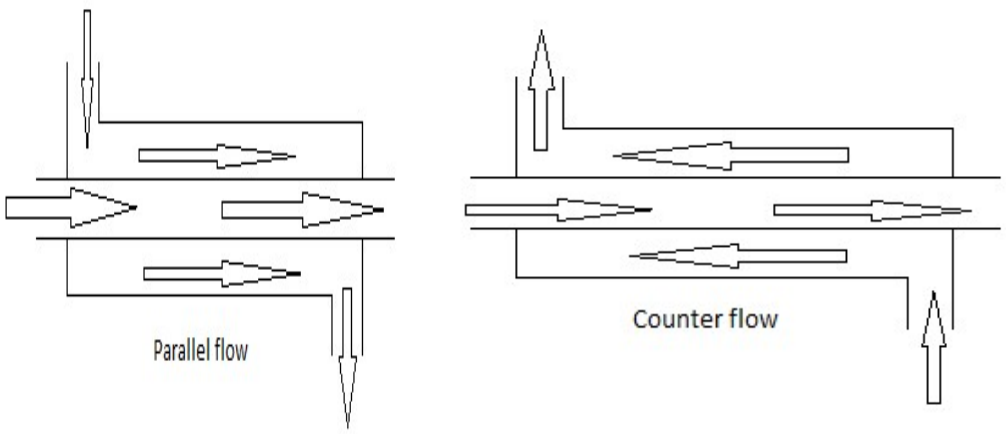

Fig. 1.1 *Parallel and Counter-flow Heat Exchanger*

2. Compact Heat Exchanger

In the compact heat exchanger, both fluids generally flow perpendicular to each other. This type of pattern is known as cross-flow. It is further categorized as mixed and unmixed flow.

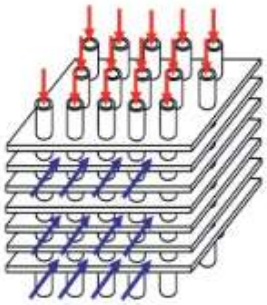

Fig. 1.2. *Compact Heat Exchanger*

3. Shell-and-Tube Heat Exchanger

This type of heat exchanger consists of a huge number of tubes packed parallel in a shell. One fluid flows inside the tubes while the second fluid flows outside the tubes. Baffles are used in the shell to increase heat transfer rate by increasing heat transfer coefficient and also used to maintain constant space between the tubes.

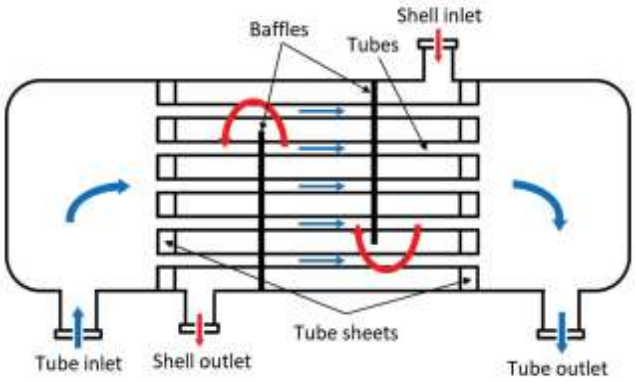

Fig. 1.3 *Shell and Tube Heat Exchanger*

4. Plate and Frame Heat Exchanger

In this type of heat exchanger, heat transfer takes place through alternate passages. It consists of several plates. Every cold fluid stream is ambiance by two hot fluid streams.

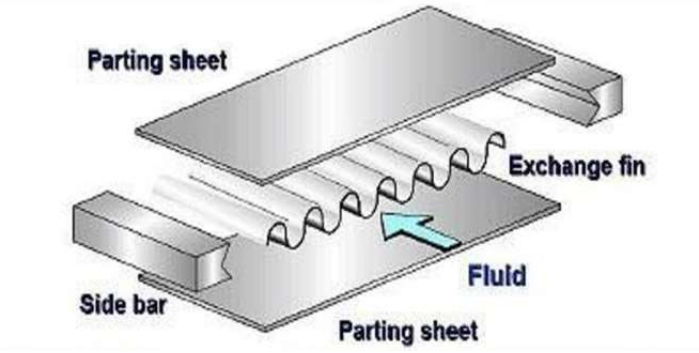

Fig. 1.4 *Plate and frame heat exchanger*

1.2 Corrosion

Corrosion is a process in which metal got degrades when it comes into the contact with the environment. It changes a metal into oxide, hydroxide, or carbonate. It generally occurs when the maximum amount of atoms on the metal surface gets oxidized. It damaged the whole surface when the metal comes in contact with air or water due to the oxidation process. In heat exchanger corrosion is a major issue, it affects its effectiveness and hence maintenance costs will be high.

In iron-based alloy, the chemical reactions takes place are shown in the equation (1.1) and (1.2):

On the anodic area,

$$Fe \rightarrow Fe^{2+} + 2e^{-} \tag{1.1}$$

On the cathodic area,

$$2H^{+} + 2e^{-} \rightarrow H_2 \tag{1.2}$$

Iron corrosion rates are controlled by this cathodic side reaction but it is a very slow process. This cathodic process can be boosted by depolarization [2].

Fig. 1.5 *Corrosion on Heat Exchanger*

Types of Corrosion

1. Uniform Corrosion

The uniform attack is also known as a general attack. It is distributed at a constant rate on the surface [3].

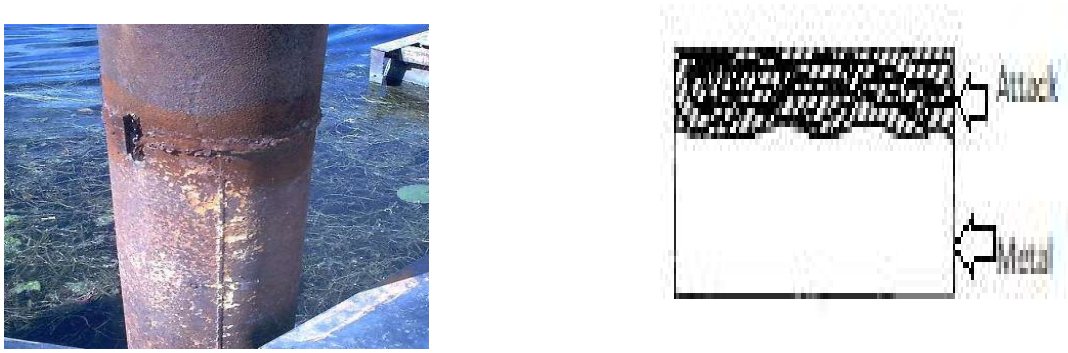

Fig. 1.6 *Uniform Corrosion*

2. Pitting Corrosion

This type of corrosion is deep and directional. It occurs during the break-in metal layer. The depth of the pits is comparatively more than their diameter [3].

Fig. 1.7 *Pitting Corrosion [3]*

3. Inter-granular corrosion

It arises along crystalline grain boundaries. It generally arises from the weld degradation of stainless steel [3].

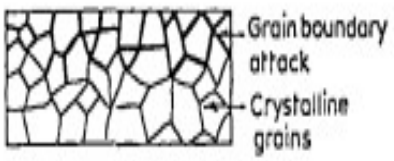

Fig.1.8 *Inter-granular corrosion [3]*

4. Crevice Corrosion

It is the form of localized corrosion in which a narrow gap in the metal surface allows leakage of liquids or air. Initiation of crevice corrosion happens due to the depletion of oxygen as well as chlorides [4].

Fig. 1.9 *Crevice corrosion [4]*

5. Stress Corrosion

Due to a combination of mechanical stress and a corrosive environment, stress corrosion comes into the picture. This type of corrosion generally occurs externally and also where the residual stress is affecting [4].

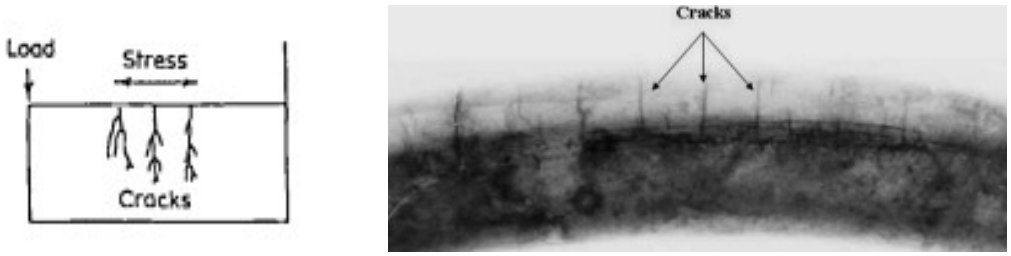

Fig. 1.10 *Stress Corrosion and Cracks [3-4]*

6. Erosion Corrosion

This type of corrosion generally occurs due to the flow of corrosive fluid on a metal surface. Due to turbulent flow, this type of corrosion can be observed. In shell and tube type heat exchanger it occurs between baffle and tube contact [4].

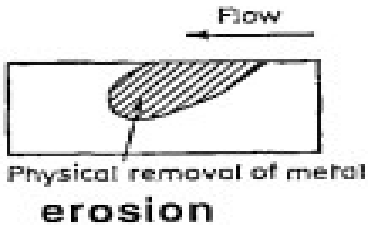

Fig. 1.11 *Erosion Corrosion [3]*

7. Galvanic Corrosion

Generally, galvanic corrosion occurs due to the electrical connection of the different types of metal and when comes into the contact with the electrolyte. The galvanic cell along with potential difference is generated due to this process [4].

Fig. 1.12 *Galvanic Corrosion*

8. Microbiologically Induced Corrosion

The bacteria, algae, and fungi are encountered when coming in contact with the environment. Very commonly these microorganisms are found in water having very low temperatures. They increase the pressure drop and also decrease the heat transfer rate [4].

Fig. 1.13 *Microbiological Corrosion*

1.3 Prevention of Corrosion

Corrosion can be prevented by changing the material to a suitable one, changing the environment where the metal is placed, using a protective coating like epoxy and polyurethane, or by modification in the design of the component [2]. Among all, the protective coating method to prevent corrosion is widely used and can be used for the long term.

Epoxy Coating

To overcome the corrosion problem, coatings are widely used nowadays due to their low cost and their compatibility. Generally, epoxy coating and polyurethane coating are used in the marine and aerospace industries. Epoxy can be used in the design of heat exchangers, but epoxy

cannot be used alone due to its low thermal conductivity and thermal capacity [5]. By using nanoparticles like graphene, we can use epoxy while designing the heat exchanger [6]. With the mixture of epoxy and graphene, it would have very good properties of thermal conductivity, thermal capacity, and anti-corrosion properties.

1.4 Motivation

In petroleum, oil, and gas industries heat exchangers play a significant role. In every process, the heat exchanger comes into contact with different types of environments. Many of them are aggressive, and some of them are not measured to be corrosive. In a recent investigation loss due to corrosion was studied by NACE (National Association of Corrosion Engineers) in 2016, the yearly global loss is approximately 2.5 trillion dollars. Earlier in 2001, it was studied that in the United States annually the amount of $276 billion expends on corrosion of all types. For power generation, in which heat exchangers are regularly used, the yearly corrosion budget is estimated to be $6.9 billion [4]. Epoxy coating is one of the best methods to reduce corrosion due to its anti-corrosion properties.

1.5 Benefits of the proposed research

The several benefits of the proposed research are:

- Graphene has exceptional anti-corrosive and durability properties.
- Graphene helps in improving the mechanical and surface properties of the coating.
- The overall thermal conductivity of epoxy and graphene coating can be improved by increasing the quantity of graphene.
- The incorporation of graphene helps in enhancing the chemical and wear resistance properties in the epoxy coatings.

1.6 Objectives

- To synthesize the nano-coatings and apply them through the paint spray technique.
- Characterize the nano-coating using FE-SEM and Raman spectroscopy technique.
- Perform the experiments on the heat exchanger test rig to evaluate the efficacy of coatings compared to the base material.
- To determine the anti-corrosive behavior of the coatings using an electrochemical technique.

CHAPTER 2

Literature Review

2.2 National

Kalidasan et al. [7] studied the drop in the non-uniformity in fluid flow in a compact heat exchanger between the header tube and lateral tube. Circular, rectangular, square, and triangular headers with different flow rates ranging between Re 1000 to 20000 are analyzed. Among all cross-sections and for different inlet mass flow rates, the triangular header is best for uniform distribution. It has been found that low mal-distribution is very high for circular cross-sectional headers and is low for triangular cross-sections when compared with other configurations.

Raja et al. [8] studied the consequence of the boundary of aluminium (Al) and stainless steel (SS) with the help of Cd, Cu, Ag, and brass interlayer. The interface is created by applying the aluminium casting over stainless steel. For heat exchangers, it is a cost-effective technique. Cu interlayer results in maximum bond strength of 112.45 MPa and for Cd, it results in a bond strength of 91.2 MPa.

Rooby et al. [9] estimated the performance of a novel Nano-phase reformed fly ash-based cement polymer coating over steel reinforcements in a corrosive atmosphere. Electrochemical studies were done with chlorides and the performance was evaluated for the long term by an impressed voltage test. Both microstructures of the coatings and chemical composition of corrosion products were analyzed using scanning electron microscopy (SEM), X-ray Diffraction technique (XRD), and Laser Raman Spectroscopic (LRS). The results show the reimbursements of Nano-material incorporated fly ash cementitious coating on rebars in corrosion protection. Corrosion rates of Nano-modified coated rebars were 76% to 89% lower than that of uncoated rebars.

Kumar et al. [10] investigate the tribological performance of dual coatings of epoxy composites. They used epoxy with 10 wt% of graphene and base oil each. Hard coatings of DLC, WC, and TiAlN were applied on D2 steel. They evaluate the coefficient of friction and wear life at 10 N and 15 N normal loads in both dry and lubricated conditions. Among all the dual-coatings at 10 N load, the COF of the dual-coating with DLC intermediate layer was the lowermost (0.09) in dry conditions. In lubricated conditions, the COF was lowest for TiAlN as

an intermediary layer (0.07). There is negligible wear on dual-coating with DLC intermediate layer under dry conditions, but there were minor scratches on the intermediate level under the base oil-lubricated state at 10 N and 15 N normal loads.

Kamde et al. [11] studied the performance of corrosion in damaged FBEC steel rebars. They studied the macro-cell corrosion specimens (Modified ASTM G 109) for Six months. Scratches on the fusion-bonded-epoxy-coating result in moisture-induced crevice corrosion. ASTM G109 test specimens can be used to assess the corrosion resistance of FBEC steel rebars.

Rajitha et al. [12] developed an efficient bio-based corrosion-resistant coating on mild steel by using gelatin. They studied the corrosion guard performance of epoxy coating integrated with modified gelatin (MGel) and MGel-graphene oxide (GO) nanocomposites on mild steel. The characterization of MGel and MGel-GO has been done using Fourier transform infrared spectroscopy (FT-IR), Raman spectroscopy, X-ray diffraction (XRD), and Thermo-gravimetric analysis (TGA). The results show the chemical interactions between GO and MGel.

2.3 International

Galeazzo et al. [13] tested both parallel and series flow arrangements by developing a flat plate with a four-channel plate heat exchanger. They compared CFD and experimental results. The CFD and experimental (plug flow model) results were quite impressive for parallel flow as compared to the series arrangement. A negligible error was found using CFD as compared to the plug flow model.

Chen et al. [14] studied the graphene-coated characteristics to improve the anti-de-icing efficiency of composite materials. The helicopter rotor is used to generate centrifugal force for conducting this experiment. The experimental data shows that graphene boosts the heat transfer of composite materials. They also studied two parameters i.e. coating thickness and spraying pressure. The thermal conductivity can be improved by reducing the coating thickness. The heat transfer is quite good while using high spraying pressure.

Sun et al. [15] studied the reduced graphene oxide in series by reducing graphene oxide thermally. They have done all experiments on different annealing temperatures from 600℃ to 1000℃ to check the thermal conductivity of epoxy composites. Better dispersion is obtained for selectively reduced graphene oxide as compared to graphene oxide.

Chen et al. [16] investigate the graphene and graphene oxide coatings with epoxy resin to improve corrosion resistance and heat transfer. The result shows that at the initial stage of the corrosion process graphene coating is better than graphene oxide. The anti-corrosion efficiency is obtained higher for graphene and graphene oxide composite coating at 0.89% mass fraction. Its anti-corrosion efficiency is 92.57% higher than neat epoxy coating. Also, the heating rate is higher for graphene and graphene oxide as compared to neat epoxy.

Li et al. [17] introduced graphene oxide fly ash cenospheres mix fillers to enhance the rust resistance of epoxy resin composite coating. They studied three types of coatings i.e. neat epoxy, epoxy resin with graphene oxide, and graphene oxide fly ash cenospheres with epoxy resin. Among three GO-FACs and epoxy resin coating is best for wear resistance. GO-FACs have better adhesion properties with epoxy resin than EP and GO/EP.

Alhumade et al. [18] studied epoxy graphene composite for rust protection coating on SS304 by using the polymerization approach. SEM and TEM are used to observe the dispersion of graphene. The results show that graphene increases the heat transfer rate and epoxy graphene coating increases the resistance to corroding.

Alhumade [19] studied the adhesion performance of epoxy graphene coating in a 3.5 wt% NaCl medium for 60 days. Post adhesion properties are analyzed by SEM. Up to 0.5% graphene gives the best results for corrosion and impact resistance for epoxy coatings.

Cui et al. [20] studied the effect on corrosion resistance by using graphene oxide with water-borne epoxy. With GO-PDA/EP there is a significant improvement in corrosion protection. Even after mechanical damages GO-PDA/EP shows better corrosion protection.

Zheng et al. [21] investigate urea-formaldehyde resin coating with modified graphene oxide. The characterization has been done with SEM, TEM, and XRD. With high dispersion of modified graphene oxide urea-formaldehyde resin and epoxy resin has superior compatibility. Results show that on carbon steel, epoxy coating and modified graphene oxide improve the corrosion protection properties.

Lin et al. [22] prepared a coating of epoxy with reduced graphene oxide and poly(styrenesulfonate) polyaniline. The mechanical and anticorrosion properties have been analyzed. PSS solution was prepared by using reduced graphene oxide platelets. Epoxy coating

at 0.5 wt% PSS-PANI/rGo improved the tensile strength by 39 % and tensile toughness by 127 % as compared to neat epoxy.

CHAPTER 3

Methodology

3.1. Materials

Stainless steel 304 is used as a coating specimen throughout the experiments. The chemical composition of SS-304 is mentioned in Table 1. Graphene powder with layer thickness: 0.8-2 nm and layer count between 1-3 with a carbon content of 85-92%, the oxygen content of 5-10% were provided by AdNano Technologies, and used for coating application. Epoxy resin with operating temperature -40 ℃ to +150 ℃ system was used to incorporate as a matrix in graphene and was procured from Electrolube India. Steel Nano guard (film thickness of 0.2-4 microns, and stables from -200℃ to +400℃ is an inorganic, eco-friendly, and water-based compound used to prevent corrosion.

Table 3.1. *Chemical composition for SS 304.*

Material	C	Mn	Si	P	S	Cr	Ni	Fe	N
%	0-0.7	0-2	0-1	0-0.5	0-0.03	17.5-19.5	8-10.5	Bal.	0-0.11

3.2 Methods

In this section, I have discussed step-by-step experimental work and the equipment that I have used while performing the experiments. Also, the characterization of graphene has been discussed briefly.

3.2.1 Preparation of the composite coatings

The coating was prepared using epoxy resin/hardener (3/1), and graphene in definite proportion. For proper dispersion, the mixture of epoxy resin and graphene was ultrasonicated for one hour in an ultrasonicator as shown in fig. 3.1(a). Stainless steel 304 plates were selected for coating with the size of 30 cm × 30 cm × 0.08 cm and 1cm × 1cm cleaned with acetone. After the acetone on the surface got evaporated, the coating was done by applying a prepared solution with a thickness of 200 microns on the SS 304 plate with the paint spray technique as shown in fig. 3.1(c) and (d). Then the coated steel plates were carried out in a vacuum drying oven at 60 ℃ for 60 minutes.

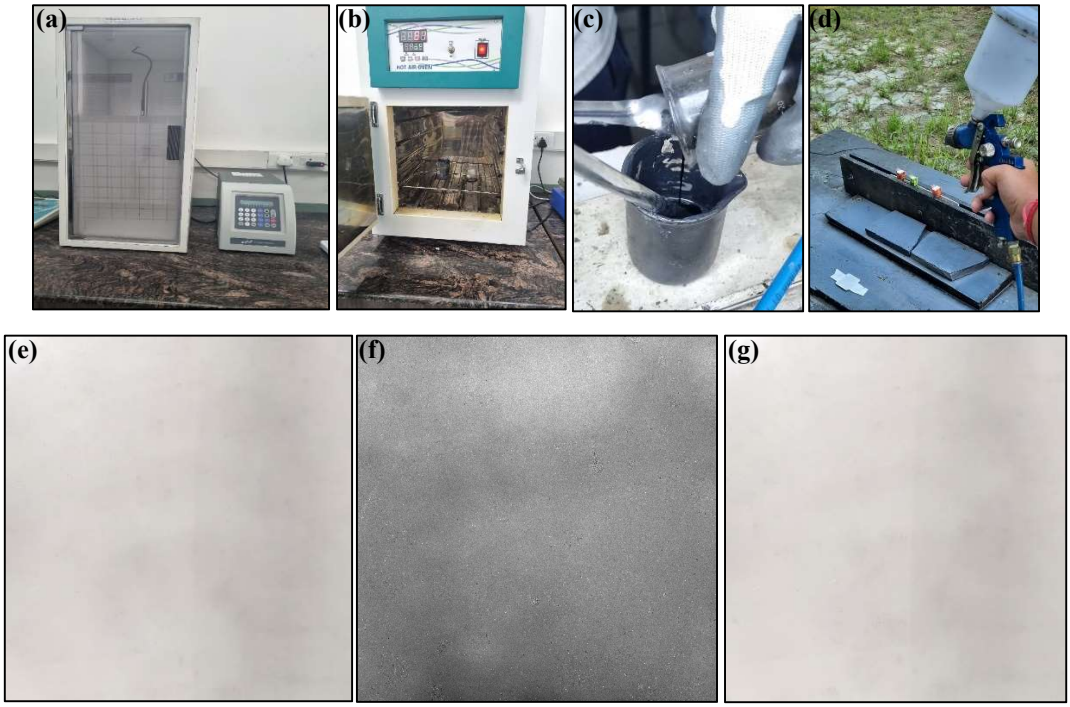

Fig. 3.1 *shows (a) Ultrasonicator (b) heat oven (c) coating preparation (d) coating with paint spray technique (e) bare steel plate (f) epoxy graphene plate (g) steel nano guard plate.*

3.2.2 Characterization

Scanning Electron Microscopy

In SEM electrons travel between an anode and electron-emitting cathode which heats the tungsten filament. The beam of a monochromatic electron is then concentrated onto the sample's surface through lenses. The beam's energy moves the electrons from atoms at the surface of the sample to either leave the surface or be adsorbed. The leaving electrons are piled up by the detector that boosts them and makes an electron micrograph [23].

With the characterization technique of Field emission scanning electron microscopy (FE-SEM, Carl Zeiss Sigma 500) we observed the morphology of the epoxy graphene coating samples. FE-SEM was used to detect the dispersion morphology and homogeneity of graphene in the epoxy resin coating and estimate the compatibility of graphene in the coatings. Before FE-SEM observation, for brittleness and reduce toughness, the coating material was solidified and vacuum dried. Then for ideal cross-section morphology, the brittle fracture was made under mechanical action.

Raman Spectroscopy

Raman spectroscopy is used to check the behavior of the vibrational mode of molecules and used to determine the numbers of graphene layers in flakes [24]. The characterization was done in the visible range of 532 nm with a power of 2.33 eV. Here, we used Raman spectra to determine the presence of graphene flakes in the epoxy graphene coating.

3.2.3 Heat Exchanger Test Rig

The heat exchanger test rig consists of one cold tank and one hot tank, two centrifugal pumps, two flow meters, and four thermo-couples. The 30×30 cm coated plate sample was held between acrylic sheets having two inlets and two outlet holes in a counter-flow heat exchanger unit as shown in Fig 3.2 (a) and (b). Every specimen experimented with three flow rates i.e 4 lpm, 6 lpm, and 8 lpm for 30 minutes each. We noted down inlet hot, inlet cold, outlet hot, and outlet temperatures every 3 minutes.

3.2.4 Water Bath

A digital water bath (MSW-273) was used to foul the coated plate as shown in fig. 3.2 (c). Every coated plate was held in the water bathtub for 7, 14, 21, and 28 days to study the effect of degrading on the epoxy-graphene coated plate.

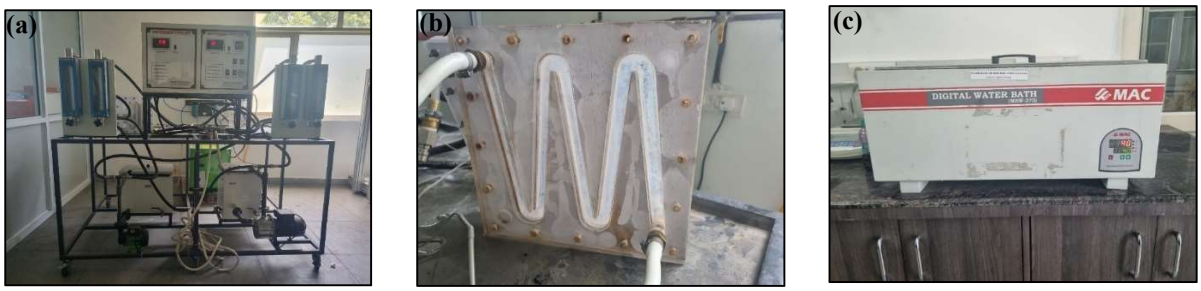

Fig. 3.2 *shows (a) heat exchanger test rig (b) acrylic sheet (c) water bath*

3.2.5 Anti-corrosion Performance Test

To evaluate the anti-corrosion performance potentiodynamic polarization tests were performed over the specimens using Gamry 1010T interface as shown in fig 3.3. Polarization studies use three-electrode cells consisting of the specimen as a working electrode, Ag/AgCl as a reference electrode, and platinum as the counter electrode. All the measurements were made at room temperature. Before conducting potentiodynamic polarization, the electrode cell was left for

30 minutes in 3.5 wt.% NaCl solution, to attain a stable open circuit potential [25]. Polarization curves were obtained at a scan rate of 1mV/sec within a potential range $\pm$ 5V relative to open circuit potential. Corrosion current density (I_{corr}), Corrosion potential (E_{corr}) were obtained from this curve using the Tafel extrapolation method including Tafel anodic (β_a) and cathodic (β_c) slope.

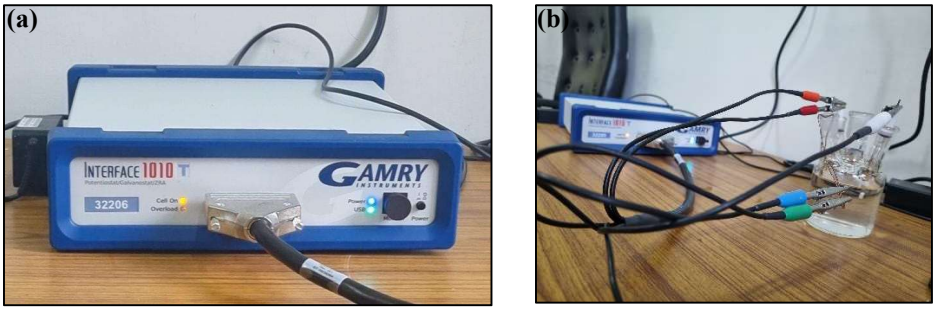

Fig 3.3 (a) *Gamry 1010T interface (b) Electrode cell*

CHAPTER 4

Results and Discussions

4.1 Microscopic Characterization

The characterization of graphene present in the coating had been done by using FE-SEM and Raman spectroscopy. In fig. 4.1 it can be noticed that the graphene is present in the epoxy coating sprayed through the HVLP spraying technique. The FE-SEM image was captured at 50,000x at an excitation voltage of 20 kV. Further, it can be concluded that epoxy-graphene-based coating is easily sprayable through the above-mentioned spraying method. Similarly, the graphene particles were observed in the Raman spectra at 50x intensified visible range laser shown in fig. 4.1. Thus we can say that the Raman spectra result in good agreement with the SEM results.

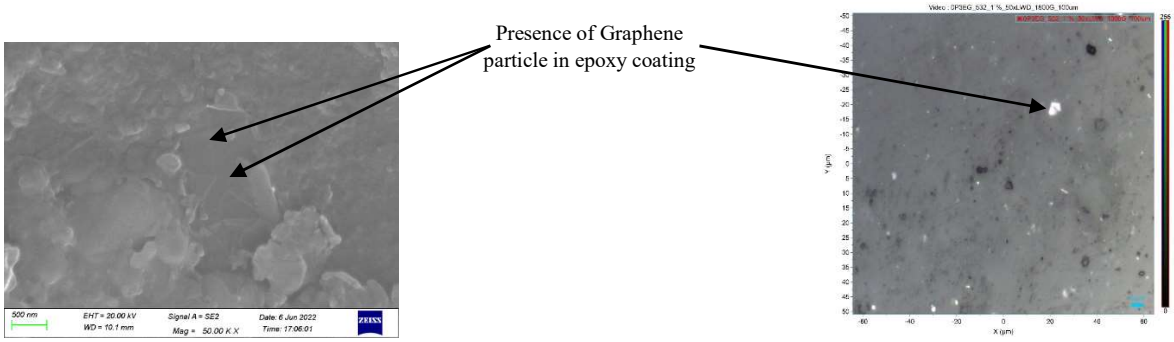

Fig. 4.1 *FE-SEM (left image) and Raman (right image) of epoxy-graphene-based coating at 50,000x magnification*

4.2 Heat Exchanger

Experiments were done on a heat exchanger test rig with different rates for 30 minutes for each bare steel, nano steel guard, and E.G wt.% 0.3 specimen. All temperature values were obtained from the test rig. After observing the temperatures LMTD, effectiveness, and overall heat transfer coefficient were calculated.

4.2.1 Calculation

Change in hot temperature: It is the temperature difference between hot fluid at the inlet to hot fluid at the outlet. Mathematically,

$$\Delta T_h = T_1 - T_2 \quad (4.1)$$

Where,

T_1 = hot water at the inlet (℃)

T_2 = hot water at the outlet (℃)

ΔT_h = change in hot temperature (℃)

Change in cold temperature: It is the temperature difference between cold fluid at the outlet to cold fluid at the inlet. Mathematically,

$$\Delta T_c = T_3 - T_4 \quad (4.2)$$

Where,

T3 = cold water at the outlet (℃)

T4 = cold water at the inlet (℃)

ΔT_c = change in cold temperature (℃)

Surface area: It is the product of the length of the plate and the height of the plate.

Mathematically,

$$A_s = L \times H \quad (4.3)$$

Where,

A_s = surface area of plate (m^2)

L = length of plate (m)

H = height of plate (m)

Cross-sectional area: It is the product of the thickness of the plate and the height of the plate.

Mathematically,

$$A_c = T \times H \quad (4.4)$$

Where,

A_c = cross-sectional area of plate (m^2)

T = thickness of plate (m)

H = height of plate (m)

Rate of heat transfer: It represents that with how much rate heat is being transferred from hot fluid to cold fluid and vice versa.

Mathematically,

$$Q_h = m_h \times C_{ph} \times \Delta T_h \quad (4.5)$$

$$Q_c = m_c \times C_{pc} \times \Delta T_c \quad (4.6)$$

Where,

Q_h = heat transfer from hot fluid (W)

Q_c = heat transfer from cold fluid (W)

m_h = mass flow rate of hot water (kg/s)

m_c = mass flow rate of cold water (kg/s)

C_{ph} = specific heat of hot water (kJ/kgK)

C_{pc} = specific heat of cold water (kJ/kgK)

Log mean temperature difference: It is a parameter that takes into account the variation of temperature difference with respect to the direction of the fluid. By averaging the variation all along the length of the heat exchanger from inlet to exit. With an increase in LMTD, the heat transfer rate is more.

Mathematically,

$$LMTD = \frac{(T_1 - T_4) - (T_2 - T_3)}{\ln((T_1 - T_4)/(T_2 - T_3))} \quad (4.7)$$

Where,

LMTD = log mean temperature difference

Overall heat transfer coefficient: This parameter considers all the modes of heat transfer in a single entity.

Mathematically,

$$U = \frac{Q_c}{A_s \times LMTD} \quad (4.8)$$

Where,

U = overall heat transfer coefficient (kW/m^{2}K)

Heat transfer effectiveness: It is defined as the ratio between the actual heat transfer rate taking place between hot and cold fluid and the maximum possible heat transfer rate that can occur between them.

Mathematically,

$$\varepsilon = \frac{Q_c}{(m \times C_p)_{min} \times (T_1 - T_3)} \tag{4.9}$$

Where,

ε = heat transfer effectiveness

4.2.2 Bare steel

From fig. 4.2 (a) initially a drop of ~3% was seen in the LMTD as the flow rate increased from 4 lpm to 8 lpm. Further, the fall in the LMTD with respect to flow rate results in the ~18% decrease in heat transfer effectiveness of the system. Similarly, after 7 days of exposure LMTD and heat transfer effectiveness decreases ~3% and ~30% respectively as shown in fig. 4.2 (b).

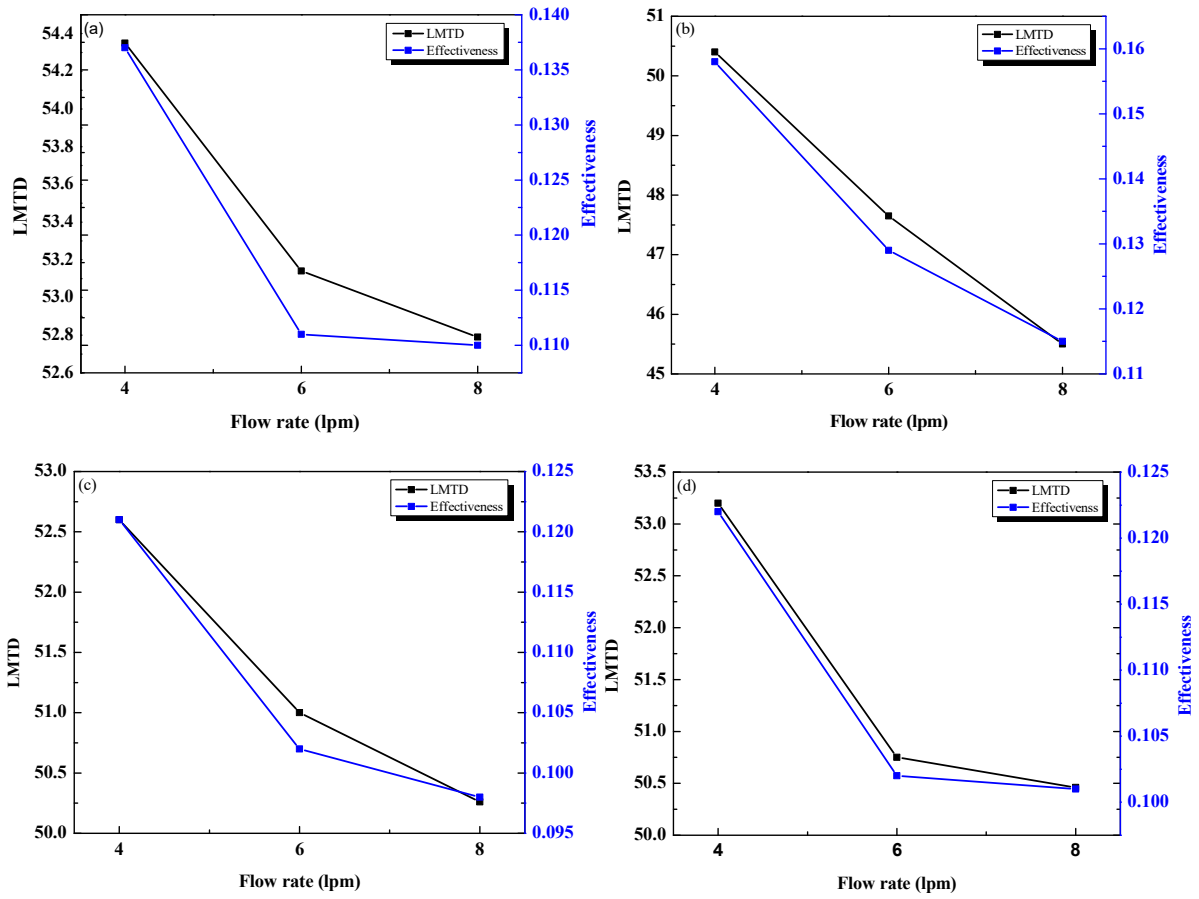

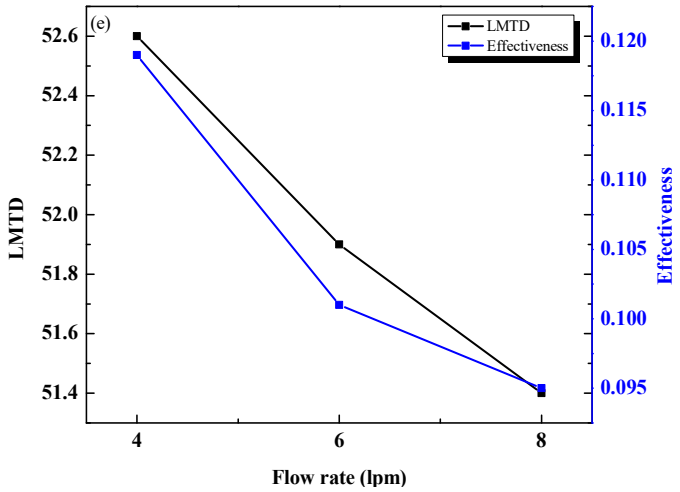

Fig. 4.2 *shows (a) bare steel initial day (b) bare steel after 7 days (c) bare steel after 14 days (d) bare steel after 21 days (e) bare steel after 28 days*

From fig. 4.2 (c) a fall of ~5% and ~20% in LMTD and heat transfer effectiveness was observed after 14 days of exposure. Further, again after 21 days of exposure, a decrease in LMTD and heat transfer effectiveness was seen as shown in fig. 4.2 (d). In fig. 4.2 (e), a similar behavior was observed in both heat transfer effectiveness and LMTD after 28 days of exposure. Thus it can be concluded from the results that the decrease in heat transfer effectiveness might be due to the presence of a scaling layer over the surface of the specimen after several days of exposure, and hence due to this decrease in heat transfer effectiveness LMTD also decreases.

4.2.3 Steel guard

In fig. 4.3 (a) initially, LMTD decreases by ~10%, and heat transfer effectiveness decreases by ~25% with the increase in mass flow rate. Further, in fig. 4.3 (b) after 7 days of exposure, it was observed that LMTD and heat transfer effectiveness reduces by ~3% and ~21%. After 14 days of exposure the drop of ~17% and ~6% in the heat transfer effectiveness and LMTD, which is evident from fig. 4.3 (c). Here, in fig. 4 (d) and (e) a similar downtrend was observed in both LMTD and heat transfer effectiveness. The variation in LMTD in heat transfer effectiveness results shows the presence of the scaling layer due to which both get decreased.

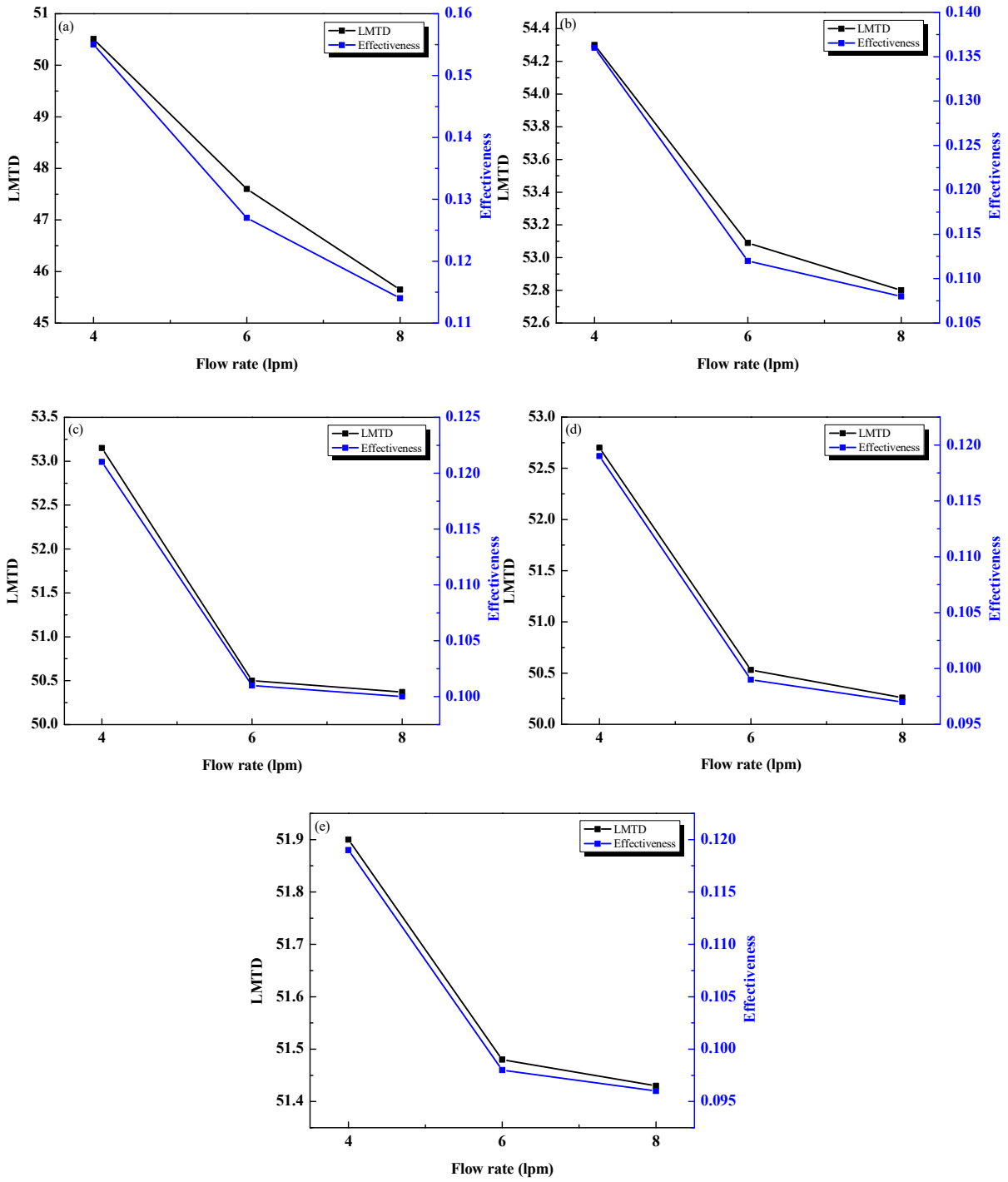

Fig. 4.3 *shows (a) Steel guard initial day (b) Steel guard after 7 days (c) Steel guard after 14 days (d) Steel guard after 21 days (e) Steel guard after 28 days*

4.2.4 Epoxy-Graphene wt.% 0.3

From fig. 4.4 (a) initially a fall of ~3% was seen in the LMTD as the flow rate increased from 4 lpm to 8 lpm. Further, the fall in the LMTD with respect to flow rate results in the ~45% drop

in heat transfer effectiveness of the system. Similarly, after 7 days of exposure LMTD and heat transfer effectiveness decreases ~2% and ~41% respectively as shown in fig. 4.4 (b).

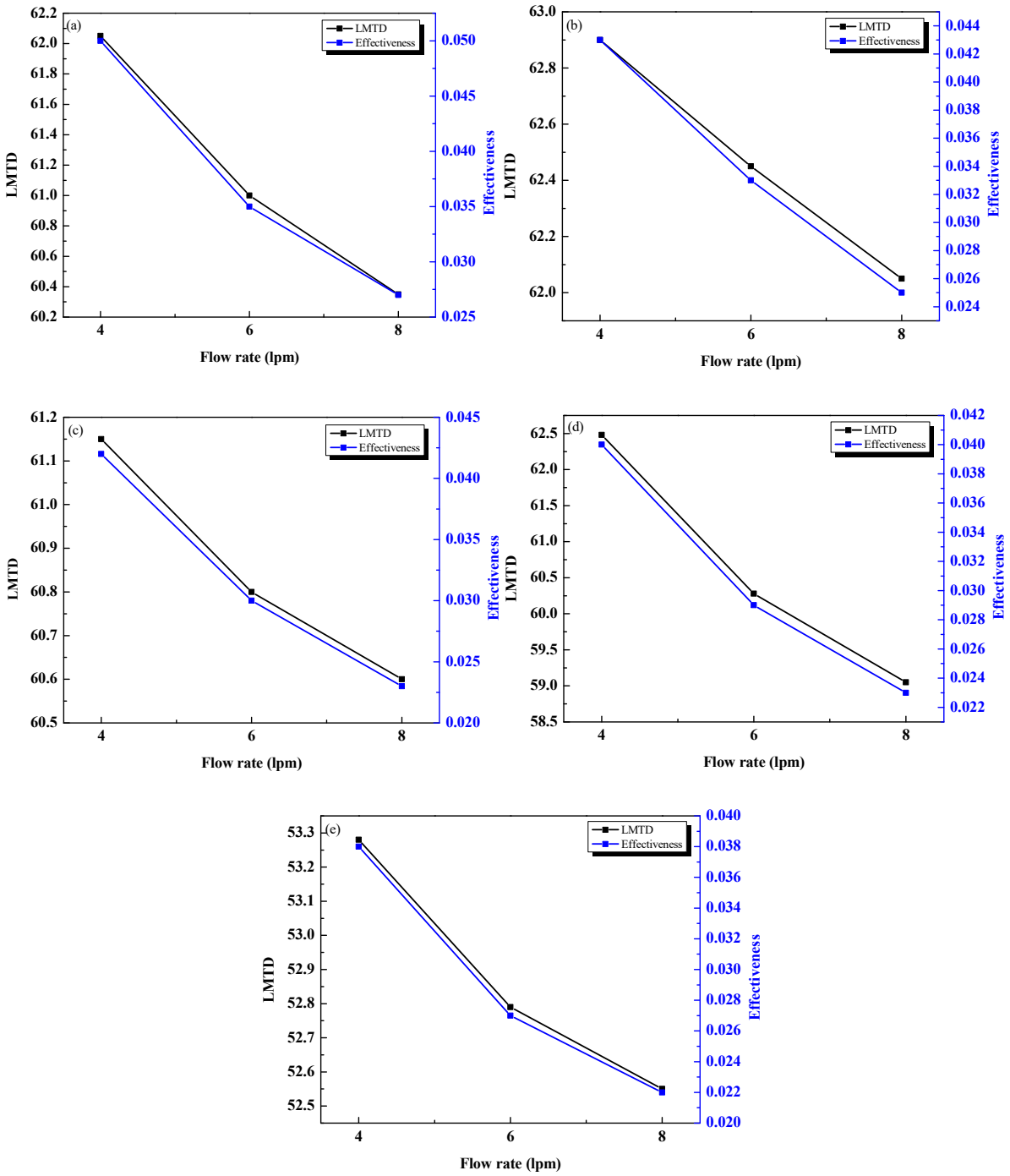

Fig. 4.4 *shows (a) E.G wt.% 0.3 initial day (b) E.G wt.% 0.3 after 7 days (c) E.G wt.% 0.3 after 14 days (d) E.G wt.% 0.3 after 21 days (e) E.G wt.% 0.3 after 28 days*

From fig. 4.4 (c) a fall of ~1% and ~45% in LMTD and heat transfer effectiveness was observed after 14 days of exposure. Further, again after 21 days of exposure, a decrease in LMTD and

heat transfer effectiveness was seen as shown in fig. 4.4 (d). In fig. 4.4 (e), a similar behavior was observed in both heat transfer effectiveness and LMTD after 28 days of exposure.

4.3 Electrochemical Corrosion Testing

Potentiodynamic tests were performed to find out the effect of corrosion on the specimen. This technique involves the change in potential of the working electrode and monitoring the current produced with respect to the change in potential of the working electrode which is the function of applied potential. After performing the polarization test, the polarization curve was plotted and electrochemical parameters like E_{corr}, I_{corr}, β_a and β_c were calculated using the Tafel extrapolation method. In fig. 4.5 (a), it was observed that with respect to applied voltage corrosion current density rises to a certain extent and then suddenly drops when the applied potential becomes zero, further rising as the voltage increases. This phenomenon occurs as the corrosion current density is the function of applied voltage. Similar behavior was observed in fig. 4.5 (b) and (c) which help to find out the electrochemical parameters.

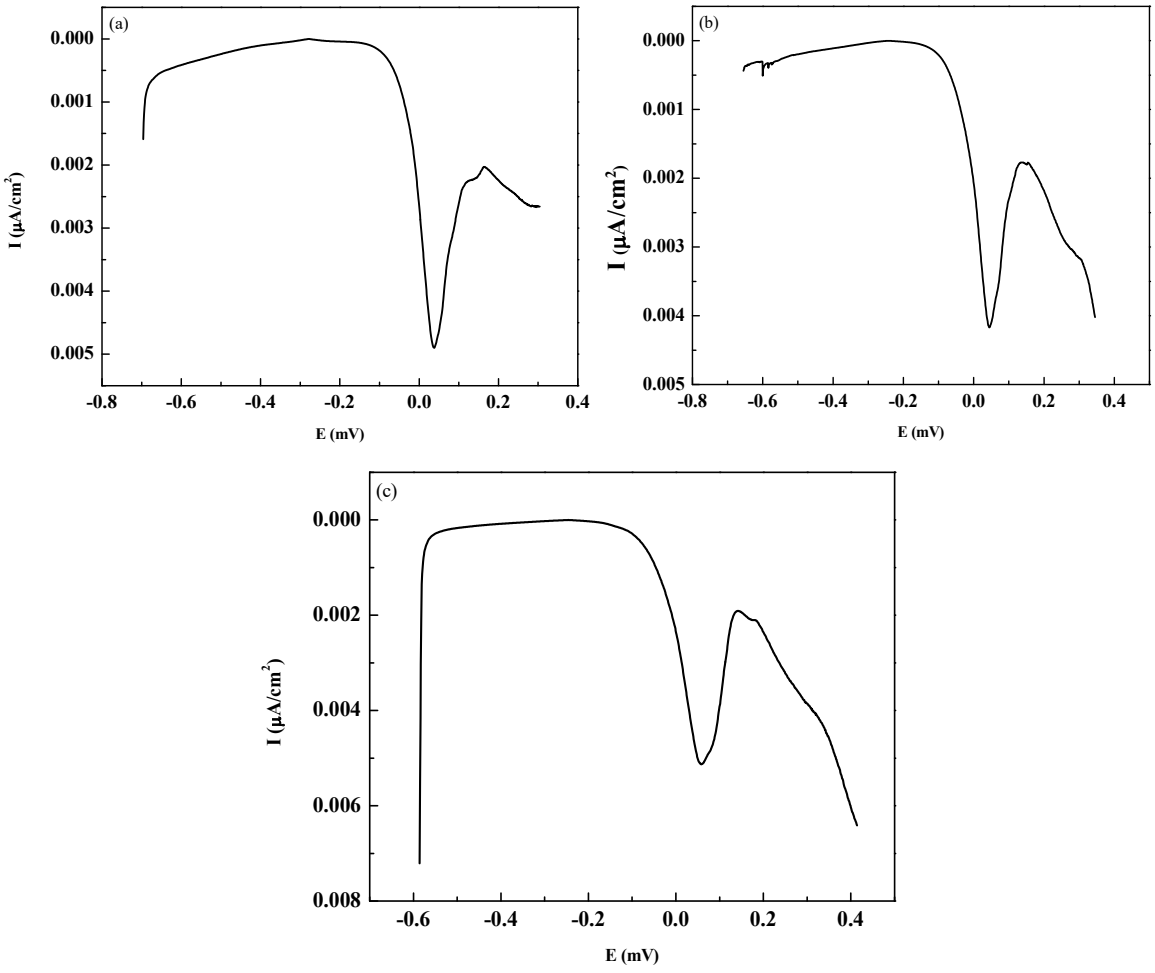

Fig. 4.5 *shows the polarization curves for (a) bare steel (b) steel guard (c) epoxy graphene wt.% 0.3*

***Table 4.1**. Electrochemical parameters*

Material	I_{corr} ($\mu A/cm^2$)	E_{corr} (mV)	β_a	β_c	R_p (Ω/cm^2)	C.R (mm/year)
Bare Steel	4.372×10^{-5}	-0.19100	1.65×10^{-4}	1.7×10^{-4}	0.83159	1.16×10^{-2}
Steel Nano guard	5.0767×10^{-5}	-0.15183	0.0012250	0.0012127	5.21235	1.34×10^{-2}
E.G 0.3%	-2.0259×10^{-4}	0.17822	-4.75×10^{-4}	-0.0535	1.00911	-5.57×10^{-2}

The electrochemical parameters like E_{corr}, I_{corr}, β_a, β_c, R_p, and C.R are listed in Table 4.1**.** The corrosion rate for bare steel is higher than the coating which shows that the bare steel is more easily corroded in nature than the epoxy graphene coating. The polarization resistance of epoxy graphene coating is better than steel nano guard coating. The steel guard coating layer vanished when came into contact with the chemical media, therefore, resulting in a high corrosion rate. Graphene is anti-corrosive due to which the incorporation of graphene in epoxy coatings exhibits excellent performance when compared to bare steel and steel guard. The Tafel extrapolation method was used to calculate the Polarization resistance (R_p) and corrosion rate (C.R.) with the help of equations given below [26].

$$R_p = \frac{\beta_a \times \beta_c}{2.303 \times (\beta_a + \beta_c) \times I_{corr}} \tag{4.10}$$

$$C.R = \frac{3.27 \times I_{corr} \times (E.W)}{D} \tag{4.11}$$

Where,

R_p = Polarization resistance

C.R. = Corrosion rate

β_a = Tafel anodic

β_c = Tafel cathodic

I_{corr} = Corrosion current density

E.W. = Equivalent weight

D = Density

CHAPTER 5
Conclusion and Future Scope

5.1 Conclusion

The heat transfer effectiveness and anti-corrosion performance of the specimens have been using a heat exchanger unit, electrochemical study, Raman, and FE-SEM analysis. From the above experimental and theoretical results, it has been concluded that:

1. In experimental results, it was seen that the heat transfer effectiveness of epoxy-graphene composite coating is reduced by 27 % and 20% respectively as compared to the bare steel and steel guard. It is also observed from electrochemical corrosion studies that in the long run epoxy graphene coated specimen exhibits anti-corrosive properties due to the presence of graphene.
2. The characterization studies like FE-SEM and Raman spectroscopy reveals the uniform distribution of graphene in the coated specimen. This confirmed that the spray coating technique is appropriate and cost effective method as compare to other popular techniques.
3. Higher resistance lowers the corrosion rate. In the electrochemical corrosion test, polarization resistance of epoxy-graphene wt.% 0.3 coating seems to be ~18% higher than the bare steel, concluding that the corrosion rate of the epoxy-graphene wt.% 0.3 coating is lesser than the base material.
4. It was also concluded that through polarization studies that the corrosion rate of epoxy-graphene wt.% 0.3 coating and bare steel is -5.57×10^{-2} mm/year and 1.16×10^{-2} mm/year, respectively, which shows that the epoxy graphene-coated specimen exhibited excellent anti-corrosive properties.

5.2 Future Scope

1. Study of variation of graphene wt. % in an epoxy matrix.
2. Studying the effects of graphene by changing graphene flakes like graphene oxide and reduced graphene oxide.
3. Studying the anticorrosion behavior of the specimen using different electrochemical techniques like electrochemical impedance spectroscopy, cyclic voltammetry, DC corrosion, etc.

References

[1] B. Zohuri, *Compact heat exchangers: Selection, application, design and evaluation*. 2016.

[2] M. Ash and I. Ash, *Handbook of Corrosion inhibitors*, vol. 98, no. 10. 2000.

[3] F. Walsh, G. Ottewill, and D. Barker, "Corrosion and protection of metals: II. Types of corrosion and protection methods," *Trans. Inst. Met. Finish.*, vol. 71, no. pt 3, pp. 117–120, 1993, doi: 10.1080/00202967.1993.11871002.

[4] W. Faes *et al.*, "Corrosion and corrosion prevention in heat exchangers," *Corros. Rev.*, vol. 37, no. 2, pp. 131–155, 2019, doi: 10.1515/corrrev-2018-0054.

[5] K. A. Zahidah, S. Kakooei, M. C. Ismail, and P. Bothi Raja, "Halloysite nanotubes as nanocontainer for smart coating application: A review," *Prog. Org. Coatings*, vol. 111, no. May, pp. 175–185, 2017, doi: 10.1016/j.porgcoat.2017.05.018.

[6] X. Shen, Z. Wang, Y. Wu, X. Liu, and J. K. Kim, "Effect of functionalization on thermal conductivities of graphene/epoxy composites," *Carbon N. Y.*, vol. 108, pp. 412–422, 2016, doi: 10.1016/j.carbon.2016.07.042.

[7] B. Kalidasan and M. Ravikumar, "Numerical analysis of compact heat exchanger for flow distribution," *Indian J. Sci. Technol.*, vol. 9, no. 6, 2016, doi: 10.17485/ijst/2016/v9i6/74596.

[8] V. Raja, M. Kavitha, B. Chokkalingam, and T. S. Ashraya, "Effect of Interlayers on Mechanical Properties of Aluminium Casting over Stainless Steel Pipe for Heat Exchanger Applications," *Trans. Indian Inst. Met.*, vol. 73, no. 6, pp. 1555–1560, 2020, doi: 10.1007/s12666-020-01937-5.

[9] D. R. Rooby, T. N. Kumar, M. Harilal, S. Sofia, R. P. George, and J. Philip, "Enhanced corrosion protection of reinforcement steel with nanomaterial incorporated fly ash based cementitious coating," *Constr. Build. Mater.*, vol. 275, p. 122130, 2021, doi: 10.1016/j.conbuildmat.2020.122130.

[10] V. Kumar, S. K. Sinha, and A. K. Agarwal, "Tribological studies of dual-coating (intermediate hard with top epoxy-graphene-base oil composite layers) on tool steel in dry and lubricated conditions," *Tribol. Int.*, vol. 127, pp. 10–23, 2018, doi: 10.1016/j.triboint.2018.05.011.

[11] D. K. Kamde and R. G. Pillai, "Comparison of Corrosion of Damaged Fusion-Bonded-Epoxy- Coated (FBEC) and Uncoated Steel Rebars," *71st RILEM Annu. Week ICACMS 2017*, no. September, 2017.

[12] K. Rajitha *et al.*, "Polyaniline-cerium oxide (PAni-CeO_2) coated graphene oxide for enhancement of epoxy coating corrosion protection performance on mild steel," *Prog. Org. Coatings*, vol. 137, no. January, p. 102723, 2020, doi: 10.1016/j.cej.2020.124925.

[13] F. C. C. Galeazzo, R. Y. Miura, J. A. W. Gut, and C. C. Tadini, "Experimental and numerical heat transfer in a plate heat exchanger," *Chem. Eng. Sci.*, vol. 61, no. 21, pp. 7133–7138, 2006, doi: 10.1016/j.ces.2006.07.029.

[14] L. Chen, Y. Zhang, and Q. Wu, "Effect of graphene coating on the heat transfer performance of a composite anti-deicing component," *Coatings*, vol. 7, no. 10, 2017, doi: 10.3390/coatings7100158.

[15] Y. Sun, L. Chen, J. Lin, P. Cui, M. Li, and X. Du, "Thermal conductivity of epoxy composites filled by thermally reduced graphite oxide with different reduction degree," *J. Compos. Mater.*, vol. 51, no. 12, pp. 1743–1752, 2017, doi: 10.1177/0021998317696137.

[16] L. Chen, H. Liu, Z. Liu, and Q. Song, "Thermal conductivity and anti-corrosion of epoxy resin based composite coatings doped with graphene and graphene oxide," *Compos. Part C Open Access*, vol. 5, no. March, p. 100124, 2021, doi: 10.1016/j.jcomc.2021.100124.

[17] J. Li, P. Chen, and Y. Wang, "Tribological and corrosion performance of epoxy resin composite coatings reinforced with graphene oxide and fly ash cenospheres," *J. Appl. Polym. Sci.*, vol. 138, no. 11, pp. 1–11, 2021, doi: 10.1002/app.50042.

[18] H. Alhumade, A. Yu, A. Elkamel, and L. Simon, "Optimizing corrosion protection of stainless steel 304 by Epoxy-Graphene composite using factorial experimental design," *Proc. Int. Conf. Ind. Eng. Oper. Manag.*, p. 1105, 2016.

[19] H. Alhumade, A. Yu, A. Elkamel, L. Simon, and A. Abdala, "Enhanced protective properties and UV stability of epoxy/graphene nanocomposite coating on stainless steel," *Express Polym. Lett.*, vol. 10, no. 12, pp. 1034–1046, 2016, doi: 10.3144/expresspolymlett.2016.96.

[20] M. Cui, S. Ren, H. Zhao, Q. Xue, and L. Wang, "Polydopamine coated graphene oxide for anticorrosive reinforcement of water-borne epoxy coating," *Chem. Eng. J.*, vol. 335, pp. 255–266, Mar. 2018, doi: 10.1016/j.cej.2017.10.172.

[21] H. Zheng, Y. Shao, Y. Wang, G. Meng, and B. Liu, "Reinforcing the corrosion protection property of epoxy coating by using graphene oxide–poly(urea–formaldehyde) composites," *Corros. Sci.*, vol. 123, pp. 267–277, 2017, doi: 10.1016/j.corsci.2017.04.019.

[22] Y. T. Lin *et al.*, "Improvement of mechanical properties and anticorrosion performance of epoxy coatings by the introduction of polyaniline/graphene composite," *Surf. Coatings Technol.*, vol. 374, no. November 2017, pp. 1128–1138, 2019, doi: 10.1016/j.surfcoat.2018.01.050.

[23] A. E. Vladár and V. D. Hodoroaba, *Characterization of nanoparticles by scanning electron microscopy*. Elsevier Inc., 2019.

[24] V. Kumar, A. Kumar, D. J. Lee, and S. S. Park, "Estimation of number of graphene layers using different methods: A focused review," *Materials (Basel).*, vol. 14, no. 16, 2021, doi: 10.3390/ma14164590.

[25] A. Cheng, R. Huang, J. K. Wu, and C. H. Chen, "Effect of rebar coating on corrosion resistance and bond strength of reinforced concrete," *Constr. Build. Mater.*, vol. 19, no. 5, pp. 404–412, 2005, doi: 10.1016/j.conbuildmat.2004.07.006.

[26] A. R. and B. E. Alonso, C. Andrade;C.J. Gulikers, R. Polder, R. Cigna, O. Vennesland, M. Salta, "Recommendations of RILEM TC-154-EMC: 'Electrochemical techniques for measuring metallic corrosion' Test methods for on-site corrosion rate measurement of steel reinforcement in concrete by means of the polarization resistance method," *Mater. Struct.*, vol. 37, no. 273, pp. 623–643, 2004.

Appendix A: Bare Steel Data

Initial day

Table 1: *Flow Rate 4*

Time (min)	T_1 (°C)	T_2 (°C)	T_3 (°C)	T_4 (°C)
0	70.7	62	17.4	25.7
3	76.1	66.9	18.1	27
6	78.1	68.8	19.4	28.8
9	78.9	69.1	20.3	29.6
12	79.8	69.9	21	30.2
15	80.4	70.9	21.3	31
18	80.9	71.3	21.7	31.1
21	81.4	72.1	22	31.6
24	81.7	72.2	22.2	31.8
27	82.1	72.5	22.3	31.8
30	82.5	72.6	22.4	31.9

LMTD = 50.4 °C, U = 10.51 kW/m^{2}K, ϵ = 0.158

Table 2: *Flow rate 6*

Time (min)	T_1 (°C)	T_2 (°C)	T_3 (°C)	T_4 (°C)
0	70.5	64.3	19.7	25.9
3	76.4	69	20.4	28
6	76.9	69.7	21.3	28.8
9	77.1	69.8	21.9	29.1
12	77.2	69.8	22.3	29.4
15	77.6	70.3	22.7	29.9
18	77.6	70.5	22.9	30.2
21	77.7	70.6	22.9	30.2
24	77.9	70.7	23.1	30.4
27	78.1	70.7	23.2	30.4
30	78.3	70.7	23.3	30.4

LMTD = 47.65 °C, U = 12.46 kW/m^{2}K, ϵ = 0.129

Table 3: *Flow rate 8*

Time (min)	T_1 (°C)	T_2 (°C)	T_3 (°C)	T_4 (°C)
0	70.5	65.3	16.4	23.2
3	74.8	68.8	17.7	24.6
6	74.8	69.1	21.1	27.4
9	74.8	69.1	22.5	28.6
12	74.8	69.1	23	28.9
15	74.8	69.1	23.3	29.2
18	74.8	69.1	23.5	29.3
21	74.8	69.1	23.5	29.4
24	74.8	69.1	23.5	29.4
27	74.8	69.1	23.5	29.4
30	74.8	69.1	23.5	29.4

LMTD = 45.5 °C, U = 14.46 kW/m^{2}K, ϵ = 0.115

7 days fouled

Table 4: *Flow rate 4*

Time (min)	T_1 (°C)	T_2 (°C)	T_3 (°C)	T_4 (°C)
0	70.5	63.9	20.8	27.2
3	79.7	71.3	20.9	29.3
6	81.5	73	21.4	29.8
9	82.5	74.4	21.7	30.6
12	83.3	75	21.7	30.8
15	83.9	75.2	22	30.9
18	84.4	75.2	22.9	31.5
21	84.8	75.7	23.1	31.9
24	85.8	76.3	23.1	31.9
27	86.4	77.4	23.1	31.9
30	86.4	77.4	23.2	31.9

LMTD = 54.35 °C, U = 8.92 kW/m^{2}K, ϵ = 0.137

Table 5: *Flow rate 6*

Time (min)	T_1 (°C)	T_2 (°C)	T_3 (°C)	T_4 (°C)
0	70.6	62.3	20	25.4
3	76.5	65.4	20.5	26
6	77.8	67.6	21.1	26.5
9	79	68.1	21.7	27.1
12	80.6	69.2	22.1	27.6
15	81.7	70.1	22.5	28.1
18	82.5	71.2	22.7	28.6
21	83	72.4	22.9	29
24	83.4	73.3	23.1	29.4
27	83.9	74.5	23.1	29.9
30	84.3	75.2	23.2	30

LMTD = 53.14 °C, U = 10.7 kW/m^{2}K, ϵ = 0.111

Table 6: *Flow rate 8*

Time (min)	T_1 (°C)	T_2 (°C)	T_3 (°C)	T_4 (°C)
0	70.5	62.1	19.8	25.2
3	74.6	65.3	20.5	26.1
6	75.7	66.4	21	26.6
9	76.3	67.3	21.4	27.1
12	77.2	68.2	21.9	27.5
15	78.1	69.2	22.3	27.9
18	79.1	70.3	22.7	28.3
21	80.2	71.2	23	28.7
24	81.3	72.3	23.1	29.4
27	82.5	73.4	23.2	29.8
30	83.9	74.8	23.2	29.9

LMTD = 52.79 °C, U = 14.15 kW/m^{2}K, ϵ = 0.11

14 days fouled

Table 7: *Flow rate 4*

Time (min)	T_1 (°C)	T_2 (°C)	T_3 (°C)	T_4 (°C)
0	70.6	62.9	19.8	26.2
3	73.5	65.7	20.6	26.8
6	74.6	66.9	21.3	27.4
9	75.9	68	21.8	27.9
12	77	68.9	22.2	28.5
15	78.6	70.1	22.5	28.9
18	79.8	72.2	22.9	29.6
21	81.1	73.5	23.1	30
24	82.4	74.4	23.4	30.4
27	83.4	75.5	23.4	30.7
30	84.5	76.4	23.5	31

LMTD = 53.2 °C, U = 7.86 kW/m^{2}K, ϵ = 0.122

Table 8: *Flow rate 6*

Time (min)	T_1 (°C)	T_2 (°C)	T_3 (°C)	T_4 (°C)
0	70.5	61.9	19.7	24.4
3	73.4	64.5	20.5	25.3
6	74.7	65.4	20.9	25.7
9	75.8	66.6	21.4	26.4
12	76.9	67.8	21.9	26.8
15	78.4	68.5	22.3	27.5
18	79.5	69.4	22.7	28.1
21	80.7	70.2	23.1	28.9
24	81.6	71	23.6	29.5
27	82.7	71.6	24.1	29.9
30	83.9	72.4	24.3	30.4

LMTD = 50.75 °C, U = 10.05 kW/m^{2}K, ϵ = 0.102

Table 9: *Flow rate 8*

Time (min)	T_1 (°C)	T_2 (°C)	T_3 (°C)	T_4 (°C)
0	70.5	61.8	19.9	24.9
3	73.2	64.4	20.6	25.2
6	74.6	65.3	21	25.6
9	75.6	66.5	21.5	26.3
12	76.7	67.6	21.8	26.9
15	78.5	68.3	22.2	27.6
18	79.4	69.3	22.9	28
21	80.6	70.4	23.1	28.7
24	81.7	71.2	23.5	29.4
27	82.6	71.9	24.1	30
30	83.5	72.5	24.5	30.5

LMTD = 50.46 °C, U = 13.26 kW/m^{2}K, ϵ = 0.101

After 21 days

Table 10: *Flow rate 4*

Time (min)	T_1 (°C)	T_2 (°C)	T_3 (°C)	T_4 (°C)
0	70.4	62.7	19.7	25.4
3	73.4	65.2	20.1	26.6
6	74.8	66.3	20.5	27.1
9	75.9	67.6	20.9	27.5
12	77	68.8	21.3	28
15	78.1	70	21.7	28.6
18	79.4	71.8	22.1	29.2
21	80.2	72.7	22.5	29.3
24	81.3	73.6	22.8	29.8
27	82.4	74.5	23.1	30.3
30	83.5	75.4	23.2	30.5

LMTD = 52.6 °C, U = 7.74 kW/m^{2}K, ϵ = 0.121

Table 11: *Flow rate 6*

Time (min)	T_1 (°C)	T_2 (°C)	T_3 (°C)	T_4 (°C)
0	70.5	61.9	19.7	24.4
3	74.6	64.2	20.2	26.1
6	75.3	65.4	20.6	26.5
9	76.5	66.5	21	27
12	77.7	67.8	21.4	27.6
15	79	69	21.9	28.4
18	79.9	70.1	22.3	28.9
21	80.2	71.3	22.8	29
24	81.3	72.4	23.5	29.5
27	82.5	73.3	23.9	30.1
30	83.7	74.3	24.2	30.3

LMTD = 51.01 °C, U = 9.86 kW/m^{2}K, ϵ = 0.102

Table 12: *Flow rate 8*

Time (min)	T_1 (°C)	T_2 (°C)	T_3 (°C)	T_4 (°C)
0	70.7	62.1	20.1	23.7
3	74.5	65.3	20.6	25.6
6	75.4	66.1	21.5	26
9	76.5	67.2	21.9	26.1
12	77.3	68.2	22.4	26.7
15	78.2	69.1	22.9	27.3
18	79.4	70	23.3	28.1
21	80.3	70.9	23.7	28.6
24	81.2	71.5	24.3	29.5
27	82.2	71.9	24.5	30.1
30	83.3	72.3	24.6	30.4

LMTD = 50.26 °C, U = 12.87 kW/m^{2}K, ϵ = 0.098

After 28 days

Table 13: *Flow rate 4*

Time (min)	T_1 (°C)	T_2 (°C)	T_3 (°C)	T_4 (°C)
0	70.5	62.8	20.1	25.3
3	73.6	65.3	20.5	26.5
6	74.7	66.4	20.9	27.2
9	75.8	67.7	21.3	27.4
12	77.1	68.9	21.7	28.1
15	78.2	70.1	22.1	28.5
18	79.3	71.2	22.5	29.3
21	80.4	72.8	22.8	29.4
24	81.3	73.7	23	29.7
27	82.4	74.6	23.2	30.2
30	82.5	76.4	23.3	30.4

LMTD = 52.6 °C, U = 7.53 kW/m^{2}K, ϵ = 0.119

Table 14: *Flow rate 6*

Time (min)	T_1 (°C)	T_2 (°C)	T_3 (°C)	T_4 (°C)
0	70.5	61.8	19.6	24.3
3	74.5	64.3	20.1	26
6	75.2	65.5	20.5	26.6
9	76.6	66.5	21.1	27.1
12	77.6	67.7	21.4	27.7
15	78.9	69.1	21.8	28.3
18	80	70.2	22.2	28.8
21	80.3	71.4	22.8	29.1
24	81.4	72.5	23.6	29.6
27	81.9	73.4	24	30
30	82.4	76.3	24.5	30.4

LMTD = 51.9 °C, U = 9.51 kW/m^{2}K, ϵ = 0.101

Table 15: *Flow rate 8*

Time (min)	T_1 (℃)	T_2 (℃)	T_3 (℃)	T_4 (℃)
0	70.6	62.2	20.1	23.7
3	74.4	66.2	20.6	25.6
6	75.3	67.3	21.5	26
9	76.5	68.2	21.9	26.1
12	77.2	69.2	22.4	26.7
15	78.3	70.1	22.9	27.3
18	79.3	71.9	23.3	28.1
21	80.4	72.5	23.7	28.6
24	81	73.6	24.3	29.5
27	82.2	74.8	24.5	30.1
30	82.6	76.5	25.4	30.9

LMTD = 51.4 ℃, U = 11.93 kW/m^2K, ϵ = 0.096

Appendix B: Nano-Steel Guard

Initial days

Table 18: *Flow rate 4*

Time (min)	T_1 (°C)	T_2 (°C)	T_3 (°C)	T_4 (°C)
0	70.6	62.1	17.3	25.6
3	76	66.8	18.1	27.1
6	78	68.7	19.2	28.5
9	78.8	69.2	20.1	28.9
12	79.7	70	21.1	29.3
15	80.3	70.9	21.2	29.9
18	80.8	71.4	21.8	31
21	81.3	72.2	22	31.3
24	81.6	72.3	22.3	31.5
27	82	72.4	22.4	31.6
30	82.3	72.5	22.5	31.9

LMTD = 50.51 °C, U = 10.35 kW/m^{2}K, ϵ = 0.155

Table 19: *Flow rate 6*

Time (min)	T_1 (°C)	T_2 (°C)	T_3 (°C)	T_4 (°C)
0	70.6	64.4	19.6	25.8
3	76.3	69.1	20.3	28.1
6	76.8	69.7	21.2	28.7
9	77	69.9	21.8	29
12	77.3	70.1	22.2	29.5
15	77.6	70.3	22.5	30
18	77.7	70.6	22.8	30.3
21	77.8	70.7	23	30.3
24	77.9	70.7	23.2	30.5
27	78.2	70.8	23.4	30.5
30	78.4	70.8	23.5	30.5

LMTD = 47.6 °C, U = 12.31 kW/m^{2}K, ϵ = 0.127

Table 20: *Flow rate 8*

Time (min)	T_1 (°C)	T_2 (°C)	T_3 (°C)	T_4 (°C)
0	70.4	65.4	16.3	23.1
3	75.1	68.9	17.5	24.5
6	75.1	69.3	20.9	27.3
9	75.1	69.3	22.6	28.5
12	75.1	69.3	23.1	28.8
15	75.1	69.3	23.4	29.1
18	75.1	69.3	23.6	29.4
21	75.1	69.3	23.6	29.5
24	75.1	69.3	23.6	29.5
27	75.1	69.3	23.6	29.5
30	75.1	69.3	23.6	29.5

LMTD = 45.65 °C, U = 14.41 kW/m^{2}K, ϵ = 0.114

After 7 days

Table 21: *Flow rate 4*

Time (min)	T_1 (°C)	T_2 (°C)	T_3 (°C)	T_4 (°C)
0	70.4	64	20.9	27.1
3	79.6	71.4	21	29.2
6	81.4	73.1	21.5	29.9
9	82.4	74.4	21.6	30.7
12	83.4	75.1	21.8	30.8
15	84	75.3	22.1	31
18	84.5	75.5	22.5	31.4
21	84.9	75.7	22.9	31.6
24	85.9	76.2	23.1	31.7
27	86.5	77.3	23.2	31.9
30	86.5	77.3	23.3	31.9

LMTD = 54.3 °C, U = 8.83 kW/m^{2}K, ϵ = 0.136

Table 22: *Flow rate 6*

Time (min)	T_1 (°C)	T_2 (°C)	T_3 (°C)	T_4 (°C)
0	70.7	62.3	20	25.3
3	76.6	65.5	20.4	26.1
6	77.9	67.7	20.9	26.4
9	79.1	68.2	21.5	27
12	80.5	69.3	22	27.5
15	81.6	70.2	22.5	28
18	82.6	71.3	22.8	28.5
21	83.1	72.5	23	29.1
24	83.5	73.4	23.1	29.4
27	84	74.6	23.2	29.8
30	84.4	75.3	23.4	30.1

LMTD = 53.09 °C, U = 10.55 kW/m^{2}K, ϵ = 0.112

Table 23: *Flow rate 8*

Time (min)	T_1 (°C)	T_2 (°C)	T_3 (°C)	T_4 (°C)
0	70.4	62	19.9	25.3
3	74.5	65.4	20.6	26.2
6	75.8	66.5	21.1	26.6
9	76.2	67.3	21.5	27.2
12	77.1	68.3	22	27.6
15	78.2	69.3	22.4	28
18	79	70.3	22.8	28.9
21	80.3	71.3	23.1	28.6
24	81.4	72.3	23.2	29.3
27	82.4	73.4	23.2	29.7
30	84	74.9	23.3	30

LMTD = 52.8 °C, U = 13.95 kW/m^{2}K, ϵ = 0.108

After 14 days

Table 24: *Flow rate 4*

Time (min)	T_1 (°C)	T_2 (°C)	T_3 (°C)	T_4 (°C)
0	70.5	62.8	19.7	26.3
3	73.6	65.8	20.5	26.9
6	74.6	67	21.2	27.5
9	76	67.9	21.9	28
12	77.1	68.9	22.3	28.6
15	78.5	70	22.6	29
18	79.9	72.1	23	29.7
21	81.2	73.4	23.2	30.1
24	82.5	74.5	23.5	30.5
27	83.5	75.5	23.6	30.8
30	84.6	76.5	23.7	31.1

LMTD = 53.15 °C, U = 7.76 kW/m^{2}K, ϵ = 0.121

Table 25: *Flow rate 6*

Time (min)	T_1 (°C)	T_2 (°C)	T_3 (°C)	T_4 (°C)
0	70.6	62	19.6	24.5
3	73.4	64.4	20.4	25.3
6	74.8	65.3	21	25.6
9	75.7	66.5	21.4	26.3
12	77	67.7	22	26.7
15	78.5	68.4	22.4	27.4
18	79.6	69.5	22.8	28.2
21	80.8	70.3	23.2	28.8
24	81.5	71.1	23.7	29.6
27	82.6	71.7	24.2	30
30	83.5	72.5	24.5	30.5

LMTD = 50.5 °C, U = 9.94 kW/m^{2}K, ϵ = 0.101

Table 26: *Flow rate 8*

Time (min)	T_1 (°C)	T_2 (°C)	T_3 (°C)	T_4 (°C)
0	70.6	61.9	20	25
3	73.3	64.3	20.7	25.3
6	74.5	65.4	21.1	25.7
9	75.5	66.5	21.6	26.4
12	76.8	67.5	21.9	27
15	78.6	68.2	22.3	27.5
18	79.3	69.4	23	28.1
21	80.5	70.5	23.2	28.6
24	81.8	71.3	23.6	29.3
27	82.5	72	24.1	30.1
30	83.4	72.6	24.6	30.6

LMTD = 50.37 °C, U = 13.08 kW/m^{2}K, ϵ = 0.1

After 21 days

Table 27: *Flow rate 4*

Time (min)	T_1 (°C)	T_2 (°C)	T_3 (°C)	T_4 (°C)
0	70.5	62.6	19.8	25.5
3	73.5	65.3	20.2	26.7
6	74.7	66.2	20.6	27
9	76	67.5	21	27.4
12	76.9	68.7	21.4	27.9
15	78.2	70.1	21.7	28.4
18	79.5	71.9	22	29
21	80.2	72.6	22.4	29.4
24	81.4	73.7	22.7	29.9
27	82.5	74.6	23	30.4
30	83.4	75.6	23.3	30.5

LMTD = 52.7 °C, U = 7.63 kW/m^{2}K, ϵ = 0.119

Table 28: *Flow rate 6*

Time (min)	T_1 (°C)	T_2 (°C)	T_3 (°C)	T_4 (°C)
0	70.6	61.8	20.1	24.3
3	74.5	64.1	20.5	26
6	75.2	65.3	21.1	26.6
9	76.4	66.6	21.5	27.1
12	77.6	67.9	22	27.5
15	79	69	22.4	28.5
18	79.8	70	22.7	29
21	80.3	71.2	23.4	29.2
24	81.4	72.3	23.8	29.6
27	82.4	73.2	24.2	29.9
30	83.6	74.2	24.4	30.3

LMTD = 50.53 °C, U = 9.58 kW/m^{2}K, ϵ = 0.099

Table 29: *Flow rate 8*

Time (min)	T_1 (°C)	T_2 (°C)	T_3 (°C)	T_4 (°C)
0	70.6	62	20	25.7
3	74.4	65.4	20.7	26.1
6	75.4	66	21.6	26.3
9	76.4	67.3	22	26.8
12	77.5	68.3	22.5	27.4
15	78.1	69	23	28
18	79.5	70.1	23.4	28.5
21	80.4	70.8	23.8	29
24	81.3	71.4	24.4	29.5
27	82.3	72	24.6	30.2
30	83.3	72.4	24.7	30.4

LMTD = 50.26 °C, U = 12.65 kW/m^{2}K, ϵ = 0.097

After 28 days

Table 30: *Flow rate 4*

Time (min)	T_1 (°C)	T_2 (°C)	T_3 (°C)	T_4 (°C)
0	70.6	62.7	20	25.2
3	73.5	65.4	20.6	26.6
6	74.6	66.5	21	27.3
9	75.7	67.8	21.4	27.5
12	77.2	69	21.8	28
15	78.3	70	22	28.6
18	79.4	71.1	22.4	29.4
21	80.5	72.7	22.9	29.6
24	81.2	73.6	23.1	29.8
27	82.4	74.7	23.3	30.3
30	82.6	76.5	23.6	30.4

LMTD = 51.9 °C, U = 7.36 kW/m^{2}K, ϵ = 0.119

Table 31: *Flow rate 6*

Time (min)	T_1 (°C)	T_2 (°C)	T_3 (°C)	T_4 (°C)
0	70.6	61.9	19.7	24.4
3	74.4	64.4	20.2	26.1
6	75.3	65.6	20.6	26.7
9	76.7	66.6	21.2	28.1
12	77.5	67.8	21.5	27.8
15	79	69.2	21.9	28.2
18	80.1	70.3	22.3	28.9
21	80.4	71.5	22.9	29.2
24	81.5	73.5	23.7	29.7
27	82	73.5	24.2	30
30	82.5	76.2	24.6	30.3

LMTD = 51.48 °C, U = 9.19 kW/m^{2}K, ϵ = 0.098

Table 32: *Flow rate 8*

Time (min)	T_1 (°C)	T_2 (°C)	T_3 (°C)	T_4 (°C)
0	70.5	62.3	20.2	23.8
3	74.3	66.3	20.7	25.7
6	75.3	67.4	21.6	26.1
9	76.6	68.4	22	26.4
12	77.3	69.2	22.4	26.8
15	78.4	70.2	23	27.4
18	79.4	72	23.4	28.2
21	80.5	72.6	23.8	28.7
24	81.1	73.7	24.4	29.6
27	82.3	74.9	24.6	30.2
30	82.7	76.6	25.5	31

LMTD = 51.43 °C, U = 11.92 kW/m^{2}K, ϵ = 0.096

Appendix C: Epoxy-graphene wt.% 0.3

Initial days

Table 33: *Flow rate 4*

Time (min)	T_1 (°C)	T_2 (°C)	T_3 (°C)	T_4 (°C)
0	68	63.8	21.1	22.6
3	75.5	73.1	21.2	23.2
6	78.2	75.3	21.6	23.7
9	80	77.5	22.4	24.6
12	81.7	79.3	22.5	25.3
15	83.1	80.8	22.7	25.6
18	84.3	82	22.8	26
21	85.6	83.2	22.9	26.1
24	87	84.3	23	26.2
27	87.9	85.4	23.1	26.4
30	88.2	85.6	23.2	26.5

LMTD = 62.05 °C, U = 2.97 kW/m^{2}K, ϵ = 0.05

Table 34: *Flow rate 6*

Time (min)	T_1 (°C)	T_2 (°C)	T_3 (°C)	T_4 (°C)
0	75	72.8	23	24.3
3	81.7	80	22.4	24.1
6	83.5	81.7	21.7	23.5
9	84.4	82.5	22.8	24.4
12	85.4	83.2	23.6	25.2
15	86.1	83.9	24.1	25.8
18	86.6	84.6	24.5	26.3
21	87.2	84.9	24.5	26.5
24	87.8	85.4	24.5	26.6
27	88.2	85.8	24.5	26.7
30	88.4	86.2	24.5	26.7

LMTD = 61.01 °C, U = 3.12 kW/m^{2}K, ϵ = 0.035

Table 35: *Flow rate 8*

Time (min)	T_1 (°C)	T_2 (°C)	T_3 (°C)	T_4 (°C)
0	70.4	68.2	21.2	22.7
3	77.3	75.8	21.6	23.3
6	78.9	77.6	22.7	24
9	80.4	78.8	23.7	24.9
12	81.6	79.7	23.9	25.4
15	82.6	80.9	24.2	25.8
18	83.6	81.9	24.6	26.1
21	84.5	82.7	24.6	26.2
24	85.3	83.6	24.6	26.3
27	85.9	84.2	24.6	26.4
30	86.7	84.9	24.6	26.3

LMTD = 60.35 °C, U = 3.14 kW/m^{2}K, ϵ = 0.027

After 7 days

Table 36: *Flow rate 4*

Time (min)	T_1 (°C)	T_2 (°C)	T_3 (°C)	T_4 (°C)
0	71.2	68.5	19.7	21.3
3	78.2	75.9	19.5	21.8
6	80.4	77.7	19.7	22
9	81.8	79.2	20.3	22.9
12	82.9	80.3	21.1	23.7
15	83.9	81.6	21.8	24.2
18	84.9	82.3	22.4	24.8
21	85.9	83.1	22.7	25.1
24	86.7	84	22.8	25.2
27	87.4	84.9	23	25.6
30	88	85.1	23.1	25.9

LMTD = 62.9 °C, U = 2.52 kW/m^{2}K, ϵ = 0.043

Table 37: *Flow rate 6*

Time (min)	T_1 (°C)	T_2 (°C)	T_3 (°C)	T_4 (°C)
0	76.9	74.2	22.2	23.6
3	83.5	81.9	22.2	24.1
6	85	83.4	22.3	24.1
9	85.8	84.2	22.3	24.2
12	86	85	22.4	24.3
15	87.2	85.6	22.5	24.5
18	87.7	85.9	22.5	24.6
21	87.9	86	22.5	24.5
24	87.8	86.1	22.8	24.8
27	87.9	86.2	22.9	24.9
30	87.7	86.1	22.9	25.1

LMTD = 62.45 °C, U = 2.93 kW/m^{2}K, ϵ = 0.033

Table 38: *Flow rate 8*

Time (min)	T_1 (°C)	T_2 (°C)	T_3 (°C)	T_4 (°C)
0	77.3	75.1	22.7	22.9
3	83.8	82.5	21.2	23
6	84.8	83.7	22.3	23.8
9	85.5	84.4	23.2	24.7
12	86.1	84.7	23.5	25.2
15	86.6	85	23.7	25.2
18	87	85.4	23.7	25.3
21	87.3	85.8	23.8	25.4
24	87.7	86.2	24	25.6
27	88	86.4	24.1	25.7
30	88	86.5	24.2	25.8

LMTD = 62.05 °C, U = 2.87 kW/m^{2}K, ϵ = 0.025

After 14 days

Table 39: *Flow rate 4*

Time (min)	T_1 (°C)	T_2 (°C)	T_3 (°C)	T_4 (°C)
0	68	66.1	22.5	25.1
3	75.5	72.9	22.6	25.3
6	78.2	75.5	22.7	25
9	80.6	77.9	22.9	25.2
12	82.3	79.4	23.4	25.8
15	84	80.9	23.9	26.5
18	85.2	82.2	24.5	26.9
21	86.7	83.7	24.7	27.1
24	87.8	84.7	24.8	27.4
27	88.3	85.2	25	27.6
30	88.5	85.5	25.1	27.8

LMTD = 61.15 °C, U = 2.49 kW/m^{2}K, ϵ = 0.042

Table 40: *Flow rate 6*

Time (min)	T_1 (°C)	T_2 (°C)	T_3 (°C)	T_4 (°C)
0	71.4	68.7	24.6	26.2
3	84.2	81.9	24.9	26.7
6	85.9	83.5	24.5	26.4
9	87.2	84.9	24.8	26.7
12	87.9	85.5	25	27
15	88.3	85.9	25.2	27.2
18	88.4	86	25.3	27.3
21	88.4	86.1	25.4	27.3
24	88.4	86.1	25.3	27.3
27	88.4	86.1	25.4	27.3
30	88.5	86.2	25.5	27.4

LMTD = 60.8 °C, U = 2.61 kW/m^{2}K, ϵ = 0.03

Table 41: *Flow rate 8*

Time (min)	T_1 (°C)	T_2 (°C)	T_3 (°C)	T_4 (°C)
0	70.5	68.2	24.5	25.5
3	78.8	77.4	24.9	26
6	81	79.5	23.9	25.4
9	82.9	81.2	24.8	26.2
12	84.1	82.3	25.2	26.6
15	85.6	83.5	25.2	26.8
18	86.6	85	25.3	27
21	87.7	85.8	25.4	27.1
24	88.3	86.6	25.6	27.1
27	88.4	86.7	25.6	27.2
30	88.4	86.8	25.7	27.2

LMTD = 60.6 °C, U = 2.74 kW/m^{2}K, ϵ = 0.023

After 21 days

Table 42: *Flow rate 4*

Time (min)	T_1 (°C)	T_2 (°C)	T_3 (°C)	T_4 (°C)
0	70	66.6	25.6	27.1
3	77.2	75.2	25.8	27.4
6	79.7	77.6	25.9	27.8
9	81.4	79.3	26.1	28.1
12	83.3	80.9	26.1	28.3
15	84.3	81.9	26.2	28.5
18	85.7	83.2	26.2	28.6
21	86.7	84.1	26.2	28.7
24	87.4	84.8	26.2	28.7
27	87.5	84.9	26.2	28.7
30	87.6	84.9	26.2	28.7

LMTD = 62.48 °C, U = 2.37 kW/m^{2}K, ϵ = 0.04

Table 43: *Flow rate 6*

Time (min)	T_1 (°C)	T_2 (°C)	T_3 (°C)	T_4 (°C)
0	70	68.7	26.1	27.2
3	80	78.5	26.5	27.9
6	82.6	80.9	26.7	28.2
9	84.2	82.4	26.8	28.4
12	86	84.1	26.6	28.3
15	87.2	85.3	26.7	28.4
18	88.2	86.3	26.7	28.4
21	88.4	86.6	26.7	28.5
24	88.5	86.6	26.7	28.5
27	88.5	86.6	26.8	28.5
30	88.6	86.7	26.9	28.6

LMTD = 60.28 °C, U = 2.51 kW/m^{2}K, ϵ = 0.029

Table 44: *Flow rate 8*

Time (min)	T_1 (°C)	T_2 (°C)	T_3 (°C)	T_4 (°C)
0	70.1	69.1	26.3	27.4
3	79.4	78.5	26.1	27.3
6	81.6	80.8	26.1	27.3
9	83.7	82.7	26.3	27.5
12	85.2	84.1	26.5	27.8
15	86.6	85.4	26.5	27.8
18	87.6	86.6	26.6	27.9
21	88.4	87.2	26.6	28
24	89.3	88.1	26.6	28.1
27	90.4	88.9	26.6	28.1
30	90.5	89.1	26.6	28.1

LMTD = 59.05 °C, U = 2.68 kW/m^{2}K, ϵ = 0.023

After 28 days

Table 45: *Flow rate 4*

Time (min)	T_1 (°C)	T_2 (°C)	T_3 (°C)	T_4 (°C)
0	64.5	62.8	27.5	30.1
3	71.2	68.9	27.7	30.4
6	74.1	72.3	28	29.9
9	76.1	73.7	28	30
12	76.5	74.9	28.1	30.1
15	78.9	76.9	28.1	30.1
18	80.1	78.4	28.1	30.2
21	81.3	79.2	28.1	30.2
24	82	80.1	28.1	30.2
27	82.6	80.5	28.2	30.3
30	83.1	80.9	28.2	30.3

LMTD = 53.28 °C, U = 2.22 kW/m^{2}K, ϵ = 0.038

Table 46: *Flow rate 6*

Time (min)	T_1 (°C)	T_2 (°C)	T_3 (°C)	T_4 (°C)
0	65.1	63.7	27.3	29.5
3	71.7	70.2	27.9	30.1
6	74.2	72.8	28.1	29.7
9	77.1	75.3	28.1	29.7
12	78.6	77.1	28.2	29.8
15	80.3	78.3	28.2	29.8
18	81.3	79.7	28.2	29.8
21	81.9	80.3	28.1	29.8
24	82.6	80.8	28.2	29.8
27	83.1	81.3	28.3	29.9
30	83.3	81.5	28.4	29.9

LMTD = 52.79 °C, U = 2.35 kW/m^{2}K, ϵ = 0.027

Table 47: *Flow rate 8*

Time (min)	T_1 (°C)	T_2 (°C)	T_3 (°C)	T_4 (°C)
0	65.2	63.4	28.1	29.1
3	70.5	69.5	28.3	29.4
6	73.2	72.3	28.3	29.4
9	75.9	74.7	28.2	29.3
12	77.5	76.5	28.2	29.3
15	78.8	77.4	28.2	29.3
18	79.9	78.7	28.1	29.3
21	80.7	79.3	28.2	29.3
24	81.3	80.1	28.1	29.2
27	81.6	80.4	28	29.2
30	81.8	80.6	28.1	29.2

LMTD = 52.55 °C, U = 2.55 kW/m^2K, ϵ = 0.022

ME Thesis

by Rishav Kumar

Submission date: 29-Jul-2022 12:57PM (UTC+0530)
Submission ID: 1876489299
File name: Plag_Check.pdf (1.39M)
Word count: 5775
Character count: 28056

ME Thesis

ORIGINALITY REPORT

15%	8%	12%	%
SIMILARITY INDEX	INTERNET SOURCES	PUBLICATIONS	STUDENT PAPERS

PRIMARY SOURCES

1	Vikram Kumar, Sujeet K. Sinha, Avinash K. Agarwal. "Tribological studies of dual-coating (intermediate hard with top epoxy-graphene-base oil composite layers) on tool steel in dry and lubricated conditions", Tribology International, 2018 Publication	2%
2	lambdageeks.com Internet Source	1%
3	Kalidasan, B., and M. Ravikumar. "Numerical Analysis of Compact Heat Exchanger for Flow Distribution", Indian Journal of Science and Technology, 2016. Publication	1%
4	Kamalon Rajitha, Kikkeri Narasimha Shetty Mohana, Avvadukkam Mohanan, Ambale Murthy Madhusudhana. "Evaluation of anti-corrosion performance of modified gelatin-graphene oxide nanocomposite dispersed in epoxy coating on mild steel in saline media",	1%

Colloids and Surfaces A: Physicochemical and Engineering Aspects, 2020
Publication

5	Divya Rachel Rooby, T. Nanda Kumar, Manu Harilal, S. Sofia, R.P. George, John Philip. "Enhanced corrosion protection of reinforcement steel with nanomaterial incorporated fly ash based cementitious coating", Construction and Building Materials, 2021 Publication	1 %
6	"The Cost of Corrosion in China", Springer Science and Business Media LLC, 2019 Publication	1 %
7	Shiva Kumar, P. Dinesha, K. R. N. Sai Krishna. "Experimental and numerical analysis of cylindrical turbulators in a double pipe heat exchanger under turbulent flow conditions", Journal of Turbulence, 2019 Publication	1 %
8	Long Chen, Hui Liu, Zhanqiang Liu, Qinghua Song. "Thermal conductivity and anti-corrosion of epoxy resin based composite coatings doped with graphene and graphene oxide", Composites Part C: Open Access, 2021 Publication	1 %
9	Jianchao Li, Ping Chen, Yuan Wang, Gaoyu Wang. "Corrosion resistance of surface	1 %

texturing epoxy resin coatings reinforced with fly ash cenospheres and multiwalled carbon nanotubes", Progress in Organic Coatings, 2021
Publication

10	V. Raja, M. Kavitha, B. Chokkalingam, T. S. Ashraya. "Effect of Interlayers on Mechanical Properties of Aluminium Casting over Stainless Steel Pipe for Heat Exchanger Applications", Transactions of the Indian Institute of Metals, 2020 Publication	<1 %
11	digital.library.unt.edu Internet Source	<1 %
12	Rabia Besghaier, Leila Dhouibi, Béchir Chaouachi, Marc Jeannin. "Heat exchanger failure analysis in the simulated marine environment: Prediction of the fouling removal temperature", Engineering Failure Analysis, 2021 Publication	<1 %
13	ethesis.nitrkl.ac.in Internet Source	<1 %
14	link.springer.com Internet Source	<1 %
15	Ricardo D. Riso, Matthieu Waeles, Benoît Pernet-Coudrier, Pierre Le Corre.	<1 %

	"Determination of dissolved iron(III) in estuarine and coastal waters by adsorptive stripping chronopotentiometry (SCP)", Analytical and Bioanalytical Chemistry, 2006 Publication	
16	202.204.50.104 Internet Source	<1 %
17	spiral.imperial.ac.uk Internet Source	<1 %
18	www.scielo.br Internet Source	<1 %
19	A. Kayode Coker, Rahmat Sotudeh - Gharebagh. "Heat Transfer", Wiley, 2022 Publication	<1 %
20	www.defencemetal.com Internet Source	<1 %
21	www.isees.in Internet Source	<1 %
22	Galeazzo, F.C.C.. "Experimental and numerical heat transfer in a plate heat exchanger", Chemical Engineering Science, 20061106 Publication	<1 %
23	repository.ntu.edu.sg Internet Source	<1 %
24	www.tutorhunt.com Internet Source	<1 %

25	Pang, S.J.. "Formation, thermal stability and corrosion behavior of glassy Ti"4"5Zr"5Cu"4"5Ni"5 alloy", Intermetallics, 200705 Publication	<1 %
26	kclpure.kcl.ac.uk Internet Source	<1 %
27	www.scribd.com Internet Source	<1 %
28	Sato, N.. "The stability of localized corrosion", Corrosion Science, 199512 Publication	<1 %
29	drum.lib.umd.edu Internet Source	<1 %
30	www.coursehero.com Internet Source	<1 %
31	www.irjet.net Internet Source	<1 %
32	Kadam, Suresh N., Kailash R. Jagdeo, and M.R. Nair. "Improvement in Surface Properties of Ti6Al4V Alloy by ZrN Thin Film", International Letters of Chemistry Physics and Astronomy, 2015. Publication	<1 %
33	Sagar Paneliya, Sakshum Khanna, Umang Patel, Parth Prajapati, Indrajit Mukhopadhyay.	<1 %

"Systematic investigation on fluid flow and heat transfer characteristic of a tube equipped with variable pitch twisted tape", International Journal of Thermofluids, 2020
Publication

34	atc.udg.edu Internet Source	<1%
35	crdp.ac-reims.fr Internet Source	<1%
36	ir.lib.uwo.ca Internet Source	<1%
37	www.meiasia.com Internet Source	<1%
38	www.slideshare.net Internet Source	<1%

Exclude quotes	On	Exclude matches	< 8 words
Exclude bibliography	On		